

1 **A modeling study of the nonlinear response of fine**  
2 **particles to air pollutant emissions in the Beijing-Tianjin-**  
3 **Hebei region**

4  
5 **Bin Zhao<sup>1,2,3</sup>, Wenjing Wu<sup>1,2</sup>, Shuxiao Wang<sup>1,2</sup>, Jia Xing<sup>1,2</sup>, Xing Chang<sup>1,2</sup>, Kuo-**  
6 **Nan Liou<sup>3</sup>, Jonathan H. Jiang<sup>4</sup>, Yu Gu<sup>3</sup>, Carey Jang<sup>5</sup>, Joshua S. Fu<sup>6</sup>, Yun Zhu<sup>7</sup>,**  
7 **Jiandong Wang<sup>1,2</sup>, Jiming Hao<sup>1,2</sup>**

8 [1] School of Environment, and State Key Joint Laboratory of Environment Simulation and  
9 Pollution Control, Tsinghua University, Beijing 100084, China

10 [2] State Environmental Protection Key Laboratory of Sources and Control of Air Pollution  
11 Complex, Beijing 100084, China

12 [3] Joint Institute for Regional Earth System Science and Engineering and Department of  
13 Atmospheric and Oceanic Sciences, University of California, Los Angeles, CA 90095, USA

14 [4] Jet propulsion Laboratory, California Institute of Technology, Pasadena, CA 91109, USA

15 [5] U.S. Environmental Protection Agency, Research Triangle Park, NC 27711, USA

16 [6] Department of Civil and Environmental Engineering, University of Tennessee, Knoxville,  
17 TN 37996, United States

18 [7] School of Environmental Science and Engineering, South China University of  
19 Technology, Guangzhou 510006, China

20  
21  
22 Correspondence to: Shuxiao Wang (shxwang@tsinghua.edu.cn)

23  
24 **Abstract.**

25 The Beijing-Tianjin-Hebei (BTH) region has been suffering from the most severe fine particle  
26 (PM<sub>2.5</sub>) pollution in China, which causes serious health damage and economic loss.  
27 Quantifying the source contributions to PM<sub>2.5</sub> concentrations has been a challenging task  
28 because of the complicated non-linear relationships between PM<sub>2.5</sub> concentrations and  
29 emissions of multiple pollutants from multiple spatial regions and economic sectors. In this  
30 study, we use the Extended Response Surface Modeling (ERSM) technique to investigate the

1 nonlinear response of  $PM_{2.5}$  concentrations to emissions of multiple pollutants from different  
2 regions and sectors over the BTH region, based on over 1000 simulations by a chemical  
3 transport model (CTM). The ERSM-predicted  $PM_{2.5}$  concentrations agree well with  
4 independent CTM simulations, with correlation coefficients larger than 0.99 and mean  
5 normalized errors less than 1%. Using the ERSM technique, we find that, among all air  
6 pollutants, primary inorganic  $PM_{2.5}$  makes the largest contribution (24-36%) to  $PM_{2.5}$   
7 concentrations. The contribution of primary inorganic  $PM_{2.5}$  emissions is especially high in  
8 heavily polluted winter, and is dominated by the industry as well as residential and  
9 commercial sectors, which should be prioritized in  $PM_{2.5}$  control strategies. The total  
10 contributions of all precursors (nitrogen oxides,  $NO_x$ ; sulfur dioxides,  $SO_2$ ; ammonia,  $NH_3$ ;  
11 non-methane volatile organic compounds, NMVOC; intermediate-volatility organic  
12 compounds, IVOC; primary organic aerosol, POA) to  $PM_{2.5}$  concentrations range between 31%  
13 and 48%. Among these precursors,  $PM_{2.5}$  concentrations are primarily sensitive to the  
14 emissions of  $NH_3$ , NMVOC+IVOC, and POA. The sensitivities increase substantially for  $NH_3$   
15 and  $NO_x$ , and decrease slightly for POA and NMVOC+IVOC with the increase in the  
16 emission reduction ratio, which illustrates the nonlinear relationships between precursor  
17 emissions and  $PM_{2.5}$  concentrations. The contributions of primary inorganic  $PM_{2.5}$  emissions  
18 to  $PM_{2.5}$  concentrations are dominated by local emission sources, which account for over 75%  
19 of the total primary inorganic  $PM_{2.5}$  contributions. For precursors, however, emissions from  
20 other regions could play similar roles as local emission sources in the summer and over the  
21 northern part of BTH. The source contribution features for various types of heavy-pollution  
22 episodes are distinctly different from each other, and from the monthly mean results,  
23 illustrating that control strategies should be differentiated based on the major contributing  
24 sources during different types of episodes.

25

## 26 **1 Introduction**

27 China is one of the regions with highest concentration of  $PM_{2.5}$  (particulate matter with  
28 aerodynamic diameter equal to or less than  $2.5 \mu m$ ) in the world (van Donkelaar et al., 2015).  
29 The problem is especially serious over the Beijing-Tianjin-Hebei (BTH) region, one of the  
30 most populous and developed regions in China. Annual average  $PM_{2.5}$  concentrations in this  
31 region reached  $85-110 \mu g/m^3$  during 2013-2015, which approximately triple the standard  
32 threshold ( $35 \mu g/m^3$ ) and far exceed those in other metropolitan regions (Wang et al., 2017). It

1 has been estimated that the severe PM<sub>2.5</sub> pollution leads to about 1.05-1.23 million premature  
2 deaths per year in China (Lim et al., 2012; Burnett et al., 2014; Wang et al., 2016b), and the  
3 monetized loss over the BTH region is as high as 134 billion Chinese Yuan, representing 2.2%  
4 of regional gross domestic product (GDP) (Lv and Li, 2016). Additionally, PM<sub>2.5</sub> substantially  
5 affects global and regional climate by absorbing and scattering solar radiation and by altering  
6 cloud properties (IPCC, 2013; Seinfeld et al., 2016; Zhao et al., 2017a), which in turn exert  
7 impact on regional air quality (Wang et al., 2014a; Zhao et al., 2017b).

8 To tackle the heavy PM<sub>2.5</sub> pollution problem, Chinese government issued the "Action Plan  
9 on Prevention and Control of Air Pollution" in September 2013, which aimed at a 25%  
10 reduction in PM<sub>2.5</sub> concentrations over the BTH region by 2017 from the 2012 levels (The  
11 State Council of the People's Republic of China, 2013). The attainment of ambient PM<sub>2.5</sub>  
12 standard would further require substantial reductions in air pollutant emissions (Wang et al.,  
13 2017; Wang et al., 2015). To establish emission control strategies, many studies have  
14 apportioned the sources of PM<sub>2.5</sub> over the BTH region, either by mining monitoring data using  
15 the Positive Matrix Factorization and Chemical Mass Balance methods (e.g., Zhang et al.,  
16 2007; Yu et al., 2013) or by embedding chemical tracers in chemical transport models (CTMs)  
17 (e.g., Wang et al., 2016c; Li et al., 2015b; Ying et al., 2014). While these studies can capture  
18 the current contributions of various sources to PM<sub>2.5</sub> concentrations, these contributions could  
19 differ significantly from the PM<sub>2.5</sub> reductions induced by reducing emissions from the  
20 corresponding sources, due to highly nonlinear chemical mechanisms (Han et al., 2016; Wang  
21 et al., 2011). Therefore, it is imperative to assess the nonlinear response of PM<sub>2.5</sub> to pollutant  
22 emissions from multiple sources, which could provide direct support for the development of  
23 effective control policies.

24 The most widely used technique to evaluate the responses of PM<sub>2.5</sub> concentrations to  
25 emission changes is the "Brute force" method, which involves perturbing emissions from a  
26 certain source and repeated solution of a CTM (Russell et al., 1995). A number of studies  
27 have utilized the "Brute force" method to quantify the sensitivities of PM<sub>2.5</sub> concentrations  
28 over the BTH region to emissions from different spatial regions (Streets et al., 2007; Wang et  
29 al., 2008; Li and Han, 2016; Wang et al., 2014b) or different economic sectors (Wang et al.,  
30 2008; Han et al., 2016; Wang et al., 2014b; Liu et al., 2016), either on a seasonal basis  
31 (Streets et al., 2007; Wang et al., 2008; Han et al., 2016; Liu et al., 2016) or during a specific  
32 heavy-pollution episode (Li and Han, 2016; Wang et al., 2014b). To improve the

1 computational efficiency, several mathematic techniques embedded in CTMs have been  
2 developed to simultaneously calculate the sensitivities of the modeled concentrations to  
3 multiple emission sources, including the Decoupled Direct Method (Yang et al., 1997) and  
4 Adjoint Analysis (Sandu et al., 2005; Hakami et al., 2006). Zhang et al. (2016) used the  
5 Adjoint Analysis method to examine sensitivities of  $PM_{2.5}$  concentrations in the BTH region  
6 to pollutant emissions during several pollution periods. However, all the preceding studies  
7 only quantified first-order sensitivities and therefore could not capture the nonlinearity in the  
8 responses of  $PM_{2.5}$  concentrations to pollutant emissions, which can be extremely strong in  
9 metropolitan regions like BTH due to complex chemical mechanisms (Wang et al., 2011).  
10 Moreover, no studies have simultaneously evaluated the response of  $PM_{2.5}$  concentrations in  
11 BTH to emissions of multiple pollutants from different sectors and regions, which we need to  
12 consider and balance to develop cost-effective control strategies.

13 In light of the drawbacks of the preceding methods, the Response Surface Modeling  
14 (RSM) technique (denoted by “conventional RSM” technique hereafter to distinguish from  
15 the ERSM technique) has been developed by using advanced statistical techniques to  
16 characterize the complex nonlinear relationship between model outputs and inputs (U.S.  
17 Environmental Protection Agency, 2006; Xing et al., 2011; Wang et al., 2011). This technique  
18 has been applied to the United States (U.S. Environmental Protection Agency, 2006) and the  
19 Eastern China (Wang et al., 2011) to evaluate the response of  $PM_{2.5}$  and its chemical  
20 components to pollutant emissions. However, the number of emission scenarios required to  
21 build conventional RSM depends on the variable number via an equation of fourth or higher  
22 order (Zhao et al., 2015b). Therefore, the required scenario number would be tens of  
23 thousands for over 15 variables and even hundreds of thousands for over 25 variables, which  
24 is computationally impossible for most three-dimensional CTMs. To overcome this major  
25 limitation, we recently developed the Extended Response Surface Modeling (ERSM)  
26 technique (Zhao et al., 2015b), which substantially reduced the scenario number needed to  
27 build the response surface and hence extended its applicability to an increased number of  
28 regions, pollutants, and sectors with an acceptable computational burden.

29 Given the advantage of the ERSM technique, here we apply it to over 1000 simulations by  
30 the Community Multi-scale Air Quality model with Two-Dimensional Volatility Basis Set  
31 (CMAQ/2D-VBS) to systematically evaluate the nonlinear response of  $PM_{2.5}$  to emission  
32 changes of multiple pollutants from different sectors and regions over the BTH region. The

1 major sources contributing to  $PM_{2.5}$  and its major components are identified and the  
2 nonlinearity in the response of  $PM_{2.5}$  to emission changes is characterized. Based on results of  
3 this study, suggestions for  $PM_{2.5}$  control policies over the BTH region are proposed.

## 4 **2 Methodology**

### 5 **2.1 CMAQ/2D-VBS configuration and evaluation**

6 The CMAQ/2D-VBS model was developed in our previous study (Zhao et al., 2016) by  
7 incorporating the 2D-VBS model framework into CMAQv5.0.1. Compared with the default  
8 CMAQ, the CMAQ/2D-VBS model explicitly simulates aging of secondary organic aerosol  
9 (SOA) formed from non-methane volatile organic compounds (NMVOC), aging of primary  
10 organic aerosol (POA), and photo-oxidation of intermediate-volatility organic compounds  
11 (IVOC), thereby significantly improving the simulation results of organic aerosol (OA),  
12 particularly SOA. The model parameters within the 2D-VBS framework have been optimized  
13 in our previous studies (Zhao et al., 2015a; Zhao et al., 2016) based on a series of smog-  
14 chamber experiments. Here we use the same model parameters as those of the “High-Yield  
15 VBS” configuration reported in Zhao et al. (2016), which agrees best with surface OA and  
16 SOA observations among three model configurations. An application in the Eastern China  
17 reveals that CMAQ/2D-VBS reduces the underestimation in OA concentrations from 45%  
18 (default CMAQv5.0.1) to 19%. More importantly, while the default CMAQv5.0.1  
19 substantially underestimates the fraction of SOA in OA by 5–10 times and can not track  
20 oxygen-to-carbon ratio (O:C), the SOA fraction and O:C simulated by CMAQ/2D-VBS agree  
21 fairly well with observations.

22 We apply the CMAQ/2D-VBS model over the BTH region. One-way, double nesting  
23 simulation domains are used, as shown in Fig. 1. Domain 1 covers East Asia with a grid  
24 resolution of 36 km×36 km; domain 2 covers the BTH and its surrounding regions with a grid  
25 resolution of 12 km×12 km. We use the SAPRC99 gas-phase chemistry module and the  
26 AERO6 aerosol module, in which the treatment of OA is replaced with the 2D-VBS  
27 framework. The aerosol thermodynamics is based on ISORROPIA-II. The initial and  
28 boundary conditions for Domain 1 are kept constant as the model default profile, and those  
29 for Domain 2 are extracted from the output of Domain 1. A 5-day spin-up period is used to  
30 reduce the influence of initial conditions on modeling results.

31 The Weather Research and Forecasting Model (WRF, version 3.7) is used to generate the  
32 meteorological fields. The National Center for Environmental Prediction (NCEP)’s FNL

1 (Final) Operational Global Analysis data (ds083.2) at  $1.0^\circ \times 1.0^\circ$  and 6-h resolution are used  
2 to generate the first guess field. The NCEP's Automated Data Processing (ADP) data  
3 (ds351.0 and ds461.0) are used in objective analysis (i.e., grid nudging). The major physics  
4 options for WRF include the Kain-Fritsch cumulus scheme, the Pleim-Xiu land-surface  
5 module, the Asymmetric Convective Model with non-local upward mixing and local  
6 downward mixing (ACM2) for planetary boundary layer (PBL) parameterization, the  
7 Morrison double-moment scheme for cloud microphysics, and the Rapid Radiative Transfer  
8 Model for GCMs (RRTMG) radiation scheme. The land cover type data are obtained from the  
9 Moderate resolution Imaging Spectroradiometer (MODIS). The simulation periods are  
10 January, March, July, and October in 2014, representing winter, spring, summer, and fall. We  
11 select these four months because the occurrence frequencies of various meteorological types  
12 in these months are statistically most similar to the average conditions in winter, spring,  
13 summer, and fall during 2004-2013 (Wu, 2016).

14 A high-resolution anthropogenic emission inventory in 2014 has been developed using an  
15 "emission factor method" (Fu et al., 2013; Zhao et al., 2013b) for the BTH region by  
16 Tsinghua University. The emissions from area and mobile sources are first calculated for each  
17 prefecture-level city based on statistical data, and subsequently distributed into the model  
18 grids according to spatial distribution of population, GDP, and road networks. A unit-based  
19 method (Zhao et al., 2008) is applied to estimate and locate the emissions from large point  
20 sources (LPS) including power plants, iron and steel plants, and cement plants. The  
21 anthropogenic emission inventory in other provinces of China was originally developed for  
22 2010 and 2012 in our previous studies (Zhao et al., 2013b; Zhao et al., 2013a; Wang et al.,  
23 2014c; Cai et al., 2016), which has been updated to 2014 in this study following the same  
24 methodology. In both the BTH and national emission inventories, the emissions from open  
25 burning of agricultural residue are calculated using crop yields, straw to grain ratio, fraction  
26 of biomass burned in the open field, and emission factors (Fu et al., 2013; Zhao et al., 2013b;  
27 Wang and Zhang, 2008). We do not include the emissions from forest and grassland fires,  
28 which typically account for less than 5% of the total biomass burning emissions over the BTH  
29 region (Qin and Xie, 2011) and are not the focus of the present study. Table S1 summarizes  
30 emissions of major air pollutants in each prefecture-level city over the BTH region in 2014;  
31 Table S2 gives the provincial emissions in the whole China in 2014. The emissions for other  
32 countries are obtained from the MIX emission inventory (Li et al., 2015a) for 2010, which is

1 the latest year available. Following our previous study (Zhao et al., 2016), we assume IVOC  
2 emissions to be 30 times, 4.5 times, 1.5 times, and 3.0 times the POA emissions from gasoline  
3 vehicles, diesel vehicles, biomass burning, and other emission sources, respectively, which is  
4 based on a series of laboratory measurements (Gordon et al., 2014b; Gordon et al., 2014a;  
5 Hennigan et al., 2011; Jathar et al., 2014). The biogenic emissions were calculated by the  
6 Model of Emissions of Gases and Aerosols from Nature (MEGAN; Guenther et al., 2006).

7 We compared the simulation results of WRFv3.7 and CMAQ/2D-VBS with  
8 meteorological observations obtained from the National Climatic Data Center (NCDC), PM<sub>2.5</sub>  
9 observations at 138 state-controlled observational sites, and observations of major PM<sub>2.5</sub>  
10 chemical components at 7 sites within the modeling domain. We show that the meteorological  
11 and chemical simulations generally agree well with observations, with performance statistics  
12 mostly within the benchmark values proposed by previous studies. Details of the model  
13 evaluation methods and results are given in the Supplementary Information (Section 1, Table  
14 S3-S5, Fig. S1-S5).

## 15 **2.2 Development of ERSM prediction system**

16 The detailed methodologies of the conventional RSM and ERSM techniques have been  
17 described in our previous papers (Zhao et al., 2015b; Xing et al., 2011). Here we only  
18 summarize some key components. The conventional RSM technique characterizes the  
19 relationships between a response variable (e.g., PM<sub>2.5</sub> concentration) and a set of control  
20 variables (i.e., emissions of particular pollutants from particular sources) based on a number  
21 of randomly generated emission control scenarios (Xing et al., 2011; Wang et al., 2011). The  
22 PM<sub>2.5</sub> concentration for each emission scenario is calculated with a CTM (CMAQ/2D-VBS in  
23 this study), and the conventional RSM is subsequently established using the Maximum  
24 Likelihood Estimation - Empirical Best Linear Unbiased Predictors (MLE-EBLUPs)  
25 developed by Santner et al. (2003). Due to the limitation of the conventional RSM technique  
26 with respect to variable number, we have developed the ERSM technique (Zhao et al., 2015b)  
27 to extend the applicability to an increased number of variables and geographical regions. The  
28 ERSM technique first quantifies the relationship between PM<sub>2.5</sub> concentrations and precursor  
29 emissions for each single region using the conventional RSM technique as described above,  
30 and then assesses the effects of inter-regional transport of PM<sub>2.5</sub> and its precursors on PM<sub>2.5</sub>  
31 concentration in the target region. In order to quantify the interaction among regions, we  
32 introduce a key assumption that the emissions of precursors in the source region affect PM<sub>2.5</sub>

1 concentrations in the target region through two major processes: (1) the inter-regional  
2 transport of precursors enhancing the chemical formation of secondary  $PM_{2.5}$  in the target  
3 region; (2) the formation of secondary  $PM_{2.5}$  in the source region followed by transport to the  
4 target region. We quantify the individual contributions of these two processes as well as the  
5 contribution of local emissions in the target region, which are subsequently integrated to  
6 derive the total  $PM_{2.5}$  concentrations in the target region. The development of the ERSM  
7 prediction system requires several hundred to over 1000 emission scenarios, but once built, it  
8 enables real-time prediction of  $PM_{2.5}$  concentrations for any given control strategy and proves  
9 to be an efficient and user-friendly decision making tool. Moreover, ERSM can be applied to  
10 design least-cost control strategy once it is coupled with control cost models/functions that  
11 links the emission reductions with economic costs.

12 For application of the RSM/ERSM techniques to the BTH region, we define 5 target  
13 regions in the inner modeling domain (Domain 2), i.e., Beijing, Tianjin, Northern Hebei (N  
14 Hebei), Eastern Hebei (E Hebei), and Southern Hebei (S Hebei), as shown in Fig. 1. The  
15 decomposition of the Hebei province is based on a preliminary analysis of the pollutant  
16 transport patterns over the BTH region (Section 2 in the Supplementary Information). The  
17 simulation using back trajectory method indicates that four major types of heavy-pollution  
18 episodes in Beijing are primarily contributed by air mass from the south, the local area, the  
19 northwest, and the southeast. We develop two RSM/ERSM prediction systems (Table 1). The  
20 response variables for the first prediction system, which is built using the conventional RSM  
21 technique, are concentrations of  $PM_{2.5}$ ,  $SO_4^{2-}$ ,  $NO_3^-$ , and OA over the urban areas of  
22 prefecture-level cities in the five target regions. For the second prediction system that is  
23 established using the ERSM technique, the response variables are only  $PM_{2.5}$  concentrations.  
24 The first prediction system use 101 emission control scenarios generated by the Latin  
25 Hypercube Sample (LHS) method (Iman et al., 1980) to map atmospheric concentrations  
26 versus emissions of five  $PM_{2.5}$  precursors, i.e.,  $NO_x$ ,  $SO_2$ ,  $NH_3$ , NMVOC+IVOC, and POA, in  
27 all five target regions (Table 1). It is on one hand intended for the validation of the second  
28 system (Section 3.1), and on the other hand used to study the source contributions of major  
29  $PM_{2.5}$  components. For the second system, the emissions of the preceding  $PM_{2.5}$  precursors as  
30 well as primary inorganic  $PM_{2.5}$  (i.e., the chemical components of primary  $PM_{2.5}$  other than  
31 POA) in each of the 5 regions are categorized into 7 and 4 control variables, respectively,  
32 resulting in 55 control variables in total (Table 1). Note that we distinguish POA and primary



1 inorganic PM<sub>2.5</sub> because the former undergoes chemical reactions and produces SOA, while  
2 the latter is mostly chemically inert in the CMAQ/2D-VBS model. We generate 1121  
3 scenarios (see Table 1) to build the response surface, following the method detailed in Zhao et  
4 al. (2015b). Specifically, the scenarios include (1) 1 CMAQ/2D-VBS base case; (2) 200  
5 scenarios generated by applying LHS method for the control variables of precursors in  
6 Beijing, 200×4 scenarios generated in the same way for Tianjin, Northern Hebei, Eastern  
7 Hebei, and Southern Hebei; (3) 100 scenarios generated by applying LHS method for the total  
8 emissions of NO<sub>x</sub>, SO<sub>2</sub>, NH<sub>3</sub>, NMVOC+IVOC, and POA in all 5 regions; and (4) 20  
9 scenarios where one of the control variables of primary inorganic PM<sub>2.5</sub> emissions is set to  
10 0.25 for each scenario. Here the scenario numbers (200 in group 2 and 100 in group 3) are  
11 determined based on numerical experiments conducted in our previous studies (Xing et al.,  
12 2011; Wang et al., 2011), which showed that the response surface for 7 and 5 variables could  
13 be built with good prediction performance (mean normalized error < 1%; correlation  
14 coefficient > 0.99) using 200 and 100 scenarios, respectively. Finally, we generate 54  
15 independent scenarios for out-of-sample validation, which will be detailed in Section. 3.1.

16 For application of the ERSM prediction system to quantitatively characterize the  
17 sensitivity of PM<sub>2.5</sub> concentrations to emission changes, we define “PM<sub>2.5</sub> sensitivity” as the  
18 change ratio of PM<sub>2.5</sub> concentration divided by the reduction ratio of a emission source,  
19 following previous studies (Zhao et al., 2015b; Wang et al., 2011).

$$20 \quad S_a^X = [(C^* - C_a) / C^*] / (1 - a) \quad (4)$$

21 where  $S_a^X$  is the PM<sub>2.5</sub> sensitivity to emission source  $X$  at its emission ratio  $a$ ;  $C^*$  and  $C_a$  are  
22 PM<sub>2.5</sub> concentrations in the base case (when the emission ratio of  $X$  is 1) and in the control  
23 scenario where the emission ratio of  $X$  is  $a$ , respectively. Similar indices can be defined for  
24 chemical components of PM<sub>2.5</sub>, such as NO<sub>3</sub><sup>-</sup>, SO<sub>4</sub><sup>2-</sup>, and OA.

25

## 26 **3 Results and discussion**

### 27 **3.1 Validation of ERSM performance**

28 The conventional RSM technique has been extensively demonstrated to have high accuracy  
29 and stability in previous papers (Xing et al., 2011; Wang et al., 2011), so we only describe the  
30 validation of the ERSM technique. Following Zhao et al. (2015b), we assess the performance

1 of the ERSM prediction system using the “out-of-sample” and 2D-isopleths validation  
2 methods, which focus on the accuracy and stability of the prediction system, respectively.

3 For out-of-sample validation, we use the ERSM prediction system to calculate the PM<sub>2.5</sub>  
4 concentrations for 54 “out-of-sample” control scenarios, i.e., scenarios independent from  
5 those used to build the prediction system, and compare with the corresponding CMAQ/2D-  
6 VBS simulation results. These 54 out-of-sample scenarios (summarized in Table S6) include  
7 40 cases (case 1-40) where the control variables of precursors change but those of primary  
8 inorganic PM<sub>2.5</sub> stay the same as the base case, 4 cases (case 41-44) the other way around, and  
9 10 cases (case 45-54) where control variables of precursors and primary inorganic PM<sub>2.5</sub>  
10 change simultaneously. Most cases are generated randomly with the LHS method (case 4-6,  
11 10-12, 16-18, 22-24, 28-54), and some cases are designed where all control variables are  
12 subject to large emission changes (case 1-3, 7-9, 13-15, 19-21, 25-27).

13 Figure 2 compares the ERSM-predicted and CMAQ/2D-VBS-simulated PM<sub>2.5</sub>  
14 concentrations and PM<sub>2.5</sub> responses (defined as the difference between PM<sub>2.5</sub> concentration in  
15 an emission control scenario and that in the base case) for the out-of-sample scenarios using  
16 scatter plots. Table 2 summarizes the statistics of the model performance. The definitions of  
17 normalized error (NE), mean normalized error (MNE), and normalized mean error (NME) are  
18 given as follows:

$$19 \quad NE = |P_i - S_i| / S_i \quad (1)$$

$$20 \quad MNE = \frac{1}{N_s} \sum_{i=1}^{N_s} [|P_i - S_i| / S_i] \quad (2)$$

$$21 \quad NME = \sum_{i=1}^{N_s} |P_i - S_i| / \sum_{i=1}^{N_s} S_i \quad (3)$$

22 where  $P_i$  and  $S_i$  are the ERSM-predicted and CMAQ/2D-VBS-simulated value of the  $i^{\text{th}}$  out-  
23 of-sample scenario;  $N_s$  is the number of out-of-sample scenarios. Figure 2 shows that the  
24 ERSM predictions and CMAQ/2D-VBS simulations agree well with each other. For PM<sub>2.5</sub>  
25 concentrations, the correlation coefficients are larger than 0.99, and the MNEs and NMEs are  
26 less than 1% for all four months. The maximum NEs could be as large as 11% for particular  
27 month and region, but the 95% percentiles of NEs are all within 4.4%. NEs exceeding 4.4%  
28 happen only for the scenarios where most control variables are reduced substantially,  
29 indicating relatively large errors at low emission rates, which is consistent with our previous  
30 study (Zhao et al., 2015b). Note that all sensitivity scenarios used in Sections 3.2-3.4 have  $\leq$   
31 80% emission reductions, which helps to avoid relatively large errors. We also examine the  
32 errors in predicted PM<sub>2.5</sub> response. Since the CMAQ/2D-VBS-simulated PM<sub>2.5</sub> responses are

1 very close to zero in several scenarios, their normalized errors (NEs) and mean normalized  
2 errors (MNEs) could be extremely large even if the absolute errors are small, which cannot  
3 properly characterize the accuracy of the ERSM technique. For this reason, we only calculate  
4 the correlation coefficients and NMEs (Table 2). The correlation coefficients of PM<sub>2.5</sub>  
5 response are larger than 0.99, and the NMEs are within 5.6% for all months. In summary, the  
6 out-of-sample validation indicates an overall good agreement between ERSM predictions and  
7 CMAQ/2D-VBS simulations.

8 We further examine whether the ERSM technique can capture the trends in PM<sub>2.5</sub>  
9 concentrations in response to continuous changes in precursor emissions, i.e., the stability of  
10 the ERSM technique. To this end, we compare the 2D-isopleths of PM<sub>2.5</sub> concentrations as a  
11 function of simultaneous changes in two precursors' emissions in all five regions derived  
12 from the ERSM and conventional RSM techniques. It should be noted that, although the  
13 ERSM technique is applicable to a much larger number of control variables than conventional  
14 RSM, the assumptions in the treatment of inter-regional transport (Section 2.2) in ERSM  
15 might affect its accuracy. Nevertheless, the predictions by conventional RSM can be regarded  
16 as proxies for real CMAQ/2D-VBS simulations since it has been extensively demonstrated to  
17 have high accuracy and stability in previous studies (Xing et al., 2011; Wang et al., 2011). For  
18 this reason, the comparison between the ERSM and conventional RSM techniques helps to  
19 evaluate the stability of the ERSM technique. Figure 3 illustrates the PM<sub>2.5</sub> isopleths in  
20 Beijing as a function of three combinations of precursors, i.e., NO<sub>x</sub> vs NH<sub>3</sub>, SO<sub>2</sub> vs NH<sub>3</sub>, and  
21 VOC+IVOC vs POA; the isopleths for other regions are very similar and thus not shown. The  
22 X- and Y-axis of the figures represent the "emission ratio", defined as the ratios of the  
23 changed emissions to the emissions in the base case. For example, an emission ratio of 0.7  
24 means the emission of a particular control variable accounts for 70% that of the base case.  
25 The colour isopleths represent PM<sub>2.5</sub> concentrations. The comparison shows that the shapes of  
26 isopleths derived from both prediction systems generally agree with each other. The  
27 agreement is very good for the case of VOC+IVOC vs POA, and for the cases of NO<sub>x</sub> vs NH<sub>3</sub>  
28 and SO<sub>2</sub> vs NH<sub>3</sub> when the emission ratios for NO<sub>x</sub> and NH<sub>3</sub> are larger than 0.2. Relatively  
29 large errors occur at very low NO<sub>x</sub>/NH<sub>3</sub> emission ratios (< 0.2) due primarily to an extremely  
30 strong nonlinearity. Within these low emission ranges, the ERSM technique can capture the  
31 general trends in PM<sub>2.5</sub> concentrations in response to emission changes, but the concentration  
32 gradients predicted by ERSM are smaller than those given by conventional RSM. More

1 studies are needed to further improve the performance of ERSM at very low  $\text{NO}_x/\text{NH}_3$   
2 emission ratios. Despite the existing errors, the general consistency between RSM and  
3 ERSM-predicted isopleths demonstrates the stability of the ERSM prediction system. In other  
4 words, the discrepancies between ERSM and CMAQ/2D-VBS cannot challenge the major  
5 conclusions on the effectiveness of emission reductions. Finally, as stated in the last  
6 paragraph, all sensitivity scenarios used in the following discussions have emission ratios  $\geq$   
7 0.2, since  $< 0.2$  emission reductions are quite rare as limited by the technologically feasible  
8 reduction potentials (Wang et al., 2014c).

### 9 **3.2 Response of $\text{PM}_{2.5}$ concentrations to emissions of air pollutants**

10 Having demonstrated the reliability of the ERSM prediction system, we employ it to  
11 investigate the responses of  $\text{PM}_{2.5}$  concentrations to emissions of various pollutants from  
12 different sectors and regions. We use “ $\text{PM}_{2.5}$  sensitivity” defined in Section 2.2 to  
13 quantitatively characterize the sensitivity of  $\text{PM}_{2.5}$  concentrations to emission changes. Figure  
14 4 illustrates the sensitivity of 4-month (January, March, July, and October) mean  $\text{PM}_{2.5}$   
15 concentrations to stepped control of individual air pollutants (left panel) and individual  
16 pollutant-sector combinations (right panel) in the BTH region, which are derived from the  
17 ERSM technique. The left panel of Fig. 4 can be obtained from both the RSM and ERSM  
18 prediction systems and their results are consistent, whereas the right panel of Fig. 4, as well as  
19 the results shown in Fig. 5 and 6 can only be derived from ERSM. Among all pollutants, the  
20 4-month mean  $\text{PM}_{2.5}$  concentrations are most sensitive to the emissions of primary inorganic  
21  $\text{PM}_{2.5}$  in all five regions, and the  $\text{PM}_{2.5}$  sensitivities vary from 24% to 36% according to  
22 region. When primary inorganic  $\text{PM}_{2.5}$  emissions from various sectors are differentiated, the  
23 industry sector is found to make the largest contribution to  $\text{PM}_{2.5}$  concentrations, followed by  
24 the residential and commercial sectors; the contribution of power plants is negligibly small  
25 because of smaller emissions and higher stacks. The  $\text{PM}_{2.5}$  sensitivities to primarily inorganic  
26  $\text{PM}_{2.5}$  emissions remain constant at various reduction ratios.

27 While primary inorganic  $\text{PM}_{2.5}$  makes the largest contribution to  $\text{PM}_{2.5}$  concentrations  
28 among all air pollutants, the total contributions of all precursors ( $\text{NO}_x$ ,  $\text{SO}_2$ ,  $\text{NH}_3$ , NMVOC,  
29 IVOC, and POA), which range between 31% and 48%, exceed that of primary inorganic  
30  $\text{PM}_{2.5}$  (24-36%). Among the precursors,  $\text{PM}_{2.5}$  concentrations are primarily sensitive to the  
31 emissions of  $\text{NH}_3$ , NMVOC+IVOC, and POA, and their relative importance differ according  
32 to reduction ratio. The  $\text{PM}_{2.5}$  sensitivity to  $\text{NH}_3$  increases substantially with the increase of

1 reduction ratio, primarily attributable to the transition from NH<sub>3</sub>-rich to NH<sub>3</sub>-poor regimes  
2 when more controls are enforced. The PM<sub>2.5</sub> sensitivities to POA and NMVOC+IVOC,  
3 however, decrease slightly with the increase of reduction ratio. This is because that, based on  
4 the gas-particle absorptive partitioning theory, organics have a higher tendency to partition  
5 into the particle phase at larger OA concentrations. As a result of the nonlinearity, the PM<sub>2.5</sub>  
6 sensitivities to POA and NMVOC+IVOC emissions are larger than those to NH<sub>3</sub> emissions at  
7 small reduction ratios (e.g., 20%), while it is the other way around at large reduction ratios  
8 (e.g., 80%).

9 The PM<sub>2.5</sub> sensitivity to SO<sub>2</sub> emissions is considerably smaller compared with the three  
10 precursors above, and does not change significantly as a function of reduction ratio. From  
11 2007 to 2014 (the base year of this study), both SO<sub>2</sub> emissions and SO<sub>4</sub><sup>2-</sup> concentrations in  
12 PM<sub>2.5</sub> have been continuously decreasing due to effective control policies (Wang et al., 2017),  
13 which partly explains the small sensitivity of PM<sub>2.5</sub> to SO<sub>2</sub> emissions. The response of PM<sub>2.5</sub>  
14 concentrations to NO<sub>x</sub> emissions could change from negative to positive with the increase of  
15 reduction ratio, which has been reported in several previous studies (Dong et al., 2014; Zhao  
16 et al., 2013c; Cai et al., 2016). Small NO<sub>x</sub> emission reductions could lead to increase in O<sub>3</sub>  
17 and HO<sub>x</sub> concentrations in several seasons owing to a NMVOC-limited photochemical  
18 regime, which on one hand enhances SO<sub>4</sub><sup>2-</sup> and SOA formation, and on the other hand, could  
19 also increase NO<sub>3</sub><sup>-</sup> concentrations by accelerating the nocturnal formation of N<sub>2</sub>O<sub>5</sub> and HNO<sub>3</sub>  
20 through the NO<sub>2</sub> + O<sub>3</sub> reaction at low temperatures. A substantial reduction in NO<sub>x</sub> emissions,  
21 however, transforms the NMVOC-limited regime to a NO<sub>x</sub>-limited regime, resulting in a  
22 successive decline in concentrations of O<sub>3</sub>, HO<sub>x</sub>, and most PM<sub>2.5</sub> chemical components.  
23 Judging from the our simulation results (Fig. 4), if only the NO<sub>x</sub> emissions within the BTH  
24 region are controlled, a very large reduction ratio of about 80% is required to realize a  
25 reduction in annual PM<sub>2.5</sub> concentrations in most areas. However, the effects could be  
26 distinctly different if NO<sub>x</sub> emissions outside the BTH region are jointly reduced. Our  
27 previous studies using the CMAQ model (Zhao et al., 2013c; Wang et al., 2010; Wang et al.,  
28 2011) have shown that uniform reductions in NO<sub>x</sub> emissions in the whole China by 23-50%  
29 result in considerable annual PM<sub>2.5</sub> reduction over the BTH region. This is because NO<sub>x</sub>  
30 emission reductions in upwind regions are more likely to result in a net PM<sub>2.5</sub> decrease  
31 compared with local emission reductions, since the photochemistry typically changes from a  
32 NMVOC-limited regime in local urban areas at surface to a NO<sub>x</sub>-limited regime in downwind

1 areas or at upper levels (Xing et al., 2011). The results shown in Fig. 4 also support the above-  
2 mentioned pattern and mechanism to some extent: even a 20% NO<sub>x</sub> emission reduction in  
3 BTH can lead to PM<sub>2.5</sub> decrease in Northern Hebei, because, as the northernmost region in  
4 BTH, it is significantly affected by emissions in other regions within BTH. Note that some  
5 recently discovered chemical pathways are missing in the model, such as the oxidation of SO<sub>2</sub>  
6 by NO<sub>2</sub> in aerosol water and the SO<sub>2</sub> heterogeneous reactions on the dust surface (Fu et al.,  
7 2016; Cheng et al., 2016; Wang et al., 2016a). Incorporation of these processes in the model  
8 may affect the simulated responses of PM<sub>2.5</sub> to NO<sub>x</sub> and SO<sub>2</sub> emissions. Regarding emission  
9 sectors, the contributions of SO<sub>2</sub> and NO<sub>x</sub> emissions are dominated by “other sources” (sources  
10 other than LPS) because they emit larger amount of pollutants at lower height compared with  
11 LPS.

12 The black dotted lines in Fig. 4 show the PM<sub>2.5</sub> sensitivity when all pollutants from all  
13 sectors are controlled simultaneously. The sum of PM<sub>2.5</sub> sensitivities to individual pollutant-  
14 sector combinations (stacked columns) is mostly larger than the sensitivity to all pollutants  
15 and sectors (black dotted lines), especially under large reduction ratios. This is mainly  
16 attributed to the overlapping effect of two precursors (e.g., SO<sub>2</sub> and NH<sub>3</sub>) involved in the  
17 formation of ammonium sulfate and ammonium nitrate. Nevertheless, at small reduction  
18 ratios, the sum of individual sensitivities is sometimes smaller, because the negative effects of  
19 reducing NO<sub>x</sub> are mitigated when we simultaneously reduce NO<sub>x</sub> emissions from multiple  
20 sectors as well as emissions of other air pollutants such as NMVOC. When all pollutants and  
21 sectors are controlled together, the PM<sub>2.5</sub> sensitivity generally increases with reduction ratio,  
22 indicating that additional air quality benefit could be achieved, larger than the expectation  
23 from linear extrapolation, if more control measures are implemented.

24 Figure 5 illustrates the PM<sub>2.5</sub> sensitivities to individual pollutant-sector combinations in  
25 each month. The source contribution features are significantly discrepant in different months.  
26 The contributions of primary inorganic PM<sub>2.5</sub> emissions to PM<sub>2.5</sub> concentrations are notably  
27 higher in January than in other months, which is probably attributed to weaker dilution and  
28 slower chemical reactions in January. Regarding different emission sectors of primary  
29 inorganic PM<sub>2.5</sub>, the industrial sector plays a dominant role in all months except January,  
30 when the residential and commercial sectors make a similar or even larger contribution as  
31 compared to the industrial sector. The higher contribution of the residential and commercial  
32 sectors in January is on one hand because of the higher emissions due to heating, and on the

1 other hand explained by weaker vertical mixing in winter, which results in a larger relative  
2 contribution of low-level sources. This result highlights the importance of residential and  
3 commercial sources for PM<sub>2.5</sub> pollution controls in the winter. The contributions of precursors  
4 are dominated by POA and NMVOC+IVOC in January, while in July, NO<sub>x</sub>, SO<sub>2</sub>, and NH<sub>3</sub>,  
5 which are known to be precursors of secondary inorganic aerosols, make larger contributions  
6 than POA and NMVOC+IVOC. The responses of PM<sub>2.5</sub> concentrations to NO<sub>x</sub> emissions can  
7 be opposite in different seasons. Specifically, in July, NO<sub>x</sub> emission reductions always induce  
8 decrease in PM<sub>2.5</sub> concentrations due to a NO<sub>x</sub>-limited photochemical regime. In January,  
9 however, even a 80% reduction in NO<sub>x</sub> emissions (roughly the maximum technically feasible  
10 reduction ratio) could result in a net PM<sub>2.5</sub> increase, as a result of a strong NMVOC-limited  
11 regime. To achieve a net PM<sub>2.5</sub> reduction in January, it would be necessary to simultaneously  
12 reduce NO<sub>x</sub> emissions outside the BTH region.

13 We further evaluate the contributions of primary inorganic PM<sub>2.5</sub> and precursor emissions  
14 from various regions to PM<sub>2.5</sub> concentrations (Fig. 6, Fig. S6). Here the contributions are  
15 quantified by comparing the base case with sensitivity scenarios in which emissions from a  
16 specific source are reduced by 80%, which reaches the maximum technologically feasible  
17 reduction ratios of major pollutants in most areas (Wang et al., 2014c). Obviously, the  
18 contributions of total primary inorganic PM<sub>2.5</sub> emissions in the BTH region are dominated by  
19 local sources, which account for over 75% of the total primary inorganic PM<sub>2.5</sub> contributions.  
20 When precursor emissions are decomposed into different regions, local sources usually also  
21 represent the largest contributors, but precursor emissions from other regions (denoted by  
22 “regional precursor emissions” hereafter) could also make significant contributions,  
23 depending on regions and seasons. The precursor emissions from the northern part of BTH  
24 (e.g., Northern Hebei, Beijing) mainly contribute to local PM<sub>2.5</sub> concentrations, whereas those  
25 from the southern part of BTH (e.g., Southern Hebei) significantly affect the PM<sub>2.5</sub>  
26 concentrations in both the local region and other regions. Over the BTH, heavy pollution is  
27 frequently associated with southerly wind while strong northerly wind often blows away  
28 PM<sub>2.5</sub> pollution (Jia et al., 2008; Zheng et al., 2015), which explains the higher contribution of  
29 emissions from southern BTH to other regions. Moreover, the importance of regional  
30 precursor emissions relative to local ones is remarkably higher in July than in January, which  
31 can be explained by the southerly monsoon and stronger vertical mixing in summer that  
32 favors inter-regional transport of air pollutants. We also examine the contributions of

1 emissions outside the BTH region to PM<sub>2.5</sub> concentrations in the five target regions. The  
2 results reveal that these emissions contribute 24-33% of the 4-month mean PM<sub>2.5</sub>  
3 concentrations, among which more than 80% could be attributed to precursor emissions.  
4 Among the four months, the contribution of emissions outside BTH is considerably smaller in  
5 January (12-21%) as compared to other months (29-38%).

### 6 **3.3 Response of PM<sub>2.5</sub> chemical components to emissions of air pollutants**

7 Ambient PM<sub>2.5</sub> is comprised of complicated chemical components with distinctly different  
8 formation pathways. To gain deeper insight into the formation mechanisms and source  
9 attribution of PM<sub>2.5</sub>, we examine the sensitivities of major PM<sub>2.5</sub> components, including NO<sub>3</sub><sup>-</sup>,  
10 SO<sub>4</sub><sup>2-</sup>, and OA, to stepped control of individual air pollutants, as shown in Fig. 7 (January and  
11 July) and Fig. S7 (March and October). NO<sub>3</sub><sup>-</sup> concentrations are most sensitive to NH<sub>3</sub>  
12 emissions in all months except July, when the sensitivities of NO<sub>3</sub><sup>-</sup> concentrations to NH<sub>3</sub> and  
13 NO<sub>x</sub> emissions are similar. The NO<sub>3</sub><sup>-</sup> sensitivities to NO<sub>x</sub> emissions differ significantly  
14 according to season. In most months, NO<sub>3</sub><sup>-</sup> concentrations are positively correlated with NO<sub>x</sub>  
15 emissions. In January, however, the sensitivities of NO<sub>3</sub><sup>-</sup> concentrations to NO<sub>x</sub> emissions are  
16 mostly negative and could be positive at large reduction ratios, which can be explained by a  
17 very strong NMVOC-limited photochemical regime, and abundant ice water for  
18 heterogeneous formation of HNO<sub>3</sub> from N<sub>2</sub>O<sub>5</sub> at cold temperatures. The sensitivities of NO<sub>3</sub><sup>-</sup> to  
19 both NH<sub>3</sub> and NO<sub>x</sub> emissions show pronounced increasing trends with the increase of  
20 reduction ratio, in agreement with the strong nonlinearity in these two pollutants described in  
21 Section 3.2. NMVOC emissions make moderate positive contributions to NO<sub>3</sub><sup>-</sup>, with the  
22 largest and smallest contributions occurring in January and July in conjunction with NMVOC-  
23 limited and NO<sub>x</sub>-limited photochemical regimes, respectively. Finally, SO<sub>2</sub> emissions have  
24 very small influences on NO<sub>3</sub><sup>-</sup> concentrations.

25 For SO<sub>4</sub><sup>2-</sup>, SO<sub>2</sub> emissions represent the dominant contributor in all months. The sensitivity  
26 of SO<sub>4</sub><sup>2-</sup> concentrations to SO<sub>2</sub> emissions does not change significantly with respect to  
27 reduction ratio, consistent with the results shown in Section 3.2. The contributions of NH<sub>3</sub>  
28 emissions to SO<sub>4</sub><sup>2-</sup> concentrations are quite small except in October, when NH<sub>3</sub> accounts for  
29 approximately one fourth the contribution of SO<sub>2</sub>. NO<sub>x</sub> emissions affect SO<sub>4</sub><sup>2-</sup> concentrations  
30 mainly by altering O<sub>3</sub> and HO<sub>x</sub> concentrations, the effects of which are positive in July at  
31 large reduction ratios, and mostly negative in other months. NMVOC emissions can impose  
32 small impact on SO<sub>4</sub><sup>2-</sup> concentrations primarily through changing O<sub>3</sub> and HO<sub>x</sub> concentrations.



1 The emissions of POA and NMVOC+IVOC are obviously two major contributors to OA  
2 concentrations. The relative importance of the two is strongly dependent on season. In July,  
3 POA and NMVOC+IVOC make similar contributions to OA concentrations, while POA  
4 usually contributes more in other months. In January, the contribution of POA could account  
5 for about four times those of NMVOC+IVOC. The higher relative contribution of POA  
6 emissions in January can be explained by several reasons. First, the POA emissions are  
7 relatively higher in January due to residential heating, while the NMVOC emissions from  
8 solvent use and biogenic sources are higher in July. Second, lower temperature in winter  
9 favors the partitioning of the semi-volatile components comprising POA to the particle phase,  
10 whereas higher temperature and stronger radiation in July accelerate the formation of SOA  
11 from NMVOC+IVOC. Similar to  $\text{SO}_4^{2-}$ , the impact of  $\text{NO}_x$  emissions on OA concentrations  
12 also works through two pathways. Besides the abovementioned photochemical pathway,  $\text{NO}_x$   
13 emission reductions could lead to OA increases due to the fact that SOA yield, defined as the  
14 ratio of SOA formation to the consumption of a precursor, is generally higher at a low- $\text{NO}_x$   
15 condition than at a high- $\text{NO}_x$  condition. As an integrated effect, the responses of OA  
16 concentrations to  $\text{NO}_x$  emissions are negative in most situations.

### 17 **3.4 $\text{PM}_{2.5}$ responses to emission reductions during heavy-pollution episodes**

18 Having shown the responses of monthly-mean  $\text{PM}_{2.5}$  concentrations to pollutant emissions,  
19 we are also interested in heavy-pollution episodes, in which the source contributions could be  
20 quite different from the monthly-mean results, largely due to variations in meteorological  
21 conditions. To provide more insight into the control strategies for heavy pollution, we use the  
22 ERSM technique to investigate the source contribution features during three typical heavy-  
23 pollution episodes. We first select 47 heavy-pollution episodes over the BTH region during  
24 2013-2015 (Table S7). Subsequently, we employ the Hybrid Single Particle Lagrangian  
25 Integrated Trajectory (HYSPLIT) model (Stein et al., 2015) and Concentration Weighted  
26 Trajectory (CWT) method (Cheng et al., 2013) to identify the potential source regions for  
27  $\text{PM}_{2.5}$  during each episode, and categorize these episodes according to their source regions.  
28 We then select a representative episode from each of three most important pollution types in  
29 which the air mass primarily originates from local areas (“Local” type), from the south  
30 (“South” type), and from the southeast (“Southeast” type). We give preference to episodes  
31 within the four-month simulation period of this study to facilitate a comparison with the  
32 monthly-mean source contribution features. For this reason, we select (1) January 5-7, 2014,

1 (2) October 7-11, 2014, and (3) October 29-31, 2014 as representatives of the “Local”,  
2 “South”, and “Southeast” types. The selection of heavy-pollution episodes is detailed in  
3 Section 2 of the Supplementary Information.

4 Figure 8 shows the contribution of precursor and primary inorganic  $PM_{2.5}$  emissions from  
5 individual regions to  $PM_{2.5}$  concentrations during the three heavy-pollution episodes, and Fig.  
6 9 illustrates the sensitivity of  $PM_{2.5}$  concentrations to stepped control of individual pollutant-  
7 sector combinations. During January 5-7, 2014 (“Local” type), the contributions of local  
8 emission sources to  $PM_{2.5}$  concentrations far exceed those from other regions within BTH as  
9 well as from outside of BTH (Fig. 8). In contrast to the monthly mean results (Section 3.2),  
10 the contributions of primary inorganic  $PM_{2.5}$  emissions are comparable to, and even larger  
11 than those of precursor emissions in the BTH region. The total contributions of primary  $PM_{2.5}$   
12 (including POA) account for as high as 70-80% of the contributions of all pollutants within  
13 the BTH region, which highlights the crucial importance of primary  $PM_{2.5}$  controls during this  
14 episode. Moreover, the controls of NMVOC,  $NH_3$ , and  $SO_2$  emissions could contribute  
15 moderately to reducing  $PM_{2.5}$  concentrations. However,  $NO_X$  emission reduction induces an  
16 increase in  $PM_{2.5}$  concentrations, even at an 80% reduction ratio. Therefore, effective  
17 temporary control measures for this episode should focus on the controls of local emissions,  
18 with emphasis laid on primary  $PM_{2.5}$ .

19 During October 7-11, 2014 (“South” type), the contributions of emissions outside BTH to  
20  $PM_{2.5}$  concentrations are as large as 33% in Beijing, and 40-50% in other regions. Within the  
21 BTH region, the emissions from Southern Hebei can have similar effects to local emissions  
22 on  $PM_{2.5}$  concentrations in Beijing, indicating a strong long-range transport from the south. In  
23 addition, the total contributions of precursor emissions about double those of primary  
24 inorganic  $PM_{2.5}$  emissions. Among all precursors,  $PM_{2.5}$  concentrations are mainly sensitive to  
25 emissions of  $NH_3$ , NMVOC+IVOC, and POA. The sensitivity of  $PM_{2.5}$  concentrations to  $NO_X$   
26 emissions increases dramatically with reduction ratio. Although small  $NO_X$  reductions may  
27 slightly elevate  $PM_{2.5}$  concentrations, large  $NO_X$  emission reduction (> 50%) can result in  
28 significant  $PM_{2.5}$  reduction. To effectively mitigate  $PM_{2.5}$  pollution during this episode, we  
29 should implement control measures for precursor emissions in both the BTH region  
30 (especially the southern part) and regions south of BTH. The  $NO_X$  emissions, if controlled,  
31 should be reduced by at least 50% to avoid adverse side effect.

1 For October 29-31, 2014 (“Southeast” type), PM<sub>2.5</sub> concentrations are also significantly  
2 affected by emissions outside the BTH region. Within the BTH region, the PM<sub>2.5</sub>  
3 concentrations in Beijing and Northern Hebei are about equally affected by local emissions  
4 and emissions from Eastern Hebei and Southern Hebei, while local emissions play dominant  
5 roles in other regions. The emissions of both precursor and primary inorganic PM<sub>2.5</sub> within the  
6 BTH region make important contributions to PM<sub>2.5</sub> concentrations, and the relative  
7 significance of the two is dependent on region. All precursors except NO<sub>x</sub> can contribute  
8 considerably to PM<sub>2.5</sub> reductions, and the sensitivity of PM<sub>2.5</sub> to NH<sub>3</sub> increase rapidly with  
9 emission ratio. NO<sub>x</sub> emissions are negatively correlated with PM<sub>2.5</sub> concentrations in most  
10 cases. Regarding the temporary control strategy for this episode, it is preferable to implement  
11 joint controls of primary PM<sub>2.5</sub> and precursors both within and outside the BTH region, with  
12 stringent measures over the Eastern and Southern Hebei.

13 From the analysis above, we conclude that the source contributions are tremendously  
14 different in these three episodes, which have been demonstrated to represent some key  
15 features of the corresponding pollution types (“Local”, “South”, and “Southeast” types).  
16 Therefore, episode-specific control strategies need to be formulated based on the source  
17 contribution features of individual pollution types. Nevertheless, the results of this study are  
18 not yet sufficient to guide the development of temporary control strategies for all heavy-  
19 pollution episodes, because the conclusions drawn from the three episodes may not be  
20 generalized to pollution types. In future studies, we need to simulate more episodes to  
21 improve their classification and to comprehensively understand the source contribution  
22 features of each pollution type. For a coming heavy-pollution episode, we can predict its  
23 pollution type using an air quality forecasting model, and subsequently formulate the  
24 temporary control strategies based on the source contribution features of this specific  
25 pollution type.

#### 26 **4 Conclusion and implications**

27 In the present study, we investigated the nonlinear response of PM<sub>2.5</sub> concentrations to  
28 emission changes of multiple pollutants from different sectors and regions over the BTH  
29 region, using the ERSM technique coupled with the CMAQ/2D-VBS model.

30 Among all pollutants, primary inorganic PM<sub>2.5</sub> makes the largest contribution (24-36%) to  
31 the 4-month mean PM<sub>2.5</sub> concentrations. The contribution from primary inorganic PM<sub>2.5</sub> is  
32 especially high in heavily polluted winter, and is dominated by the industry as well as

1 residential and commercial sectors. The total contributions of all precursors to  $PM_{2.5}$   
2 concentrations range between 31% and 48%. Among the precursors,  $PM_{2.5}$  concentrations are  
3 primarily sensitive to the emissions of  $NH_3$ , NMVOC+IVOC, and POA. With the increase of  
4 reduction ratio, the sensitivities of  $PM_{2.5}$  concentrations to pollutant emissions remain roughly  
5 constant for primary inorganic  $PM_{2.5}$  and  $SO_2$ , increase substantially for  $NH_3$  and  $NO_x$ , and  
6 decrease slightly for POA and NMVOC+IVOC. The contributions of primary inorganic  $PM_{2.5}$   
7 emissions to  $PM_{2.5}$  concentrations are dominated by local emission sources, which account for  
8 over 75% of the total primary inorganic  $PM_{2.5}$  contributions. For precursors, however,  
9 emissions from other regions could play similar roles to local emission sources in the summer  
10 and over the northern part of BTH. Different  $PM_{2.5}$  chemical components are associated with  
11 distinct source contribution features. The  $NO_3^-$  and  $SO_4^{2-}$  concentrations are most sensitive to  
12 emissions of  $NH_3$  and  $SO_2$ , respectively. The emissions of the POA and NMVOC+IVOC are  
13 two major contributors to OA concentrations, with their relative importance depending on  
14 season.

15 The source contribution features are significantly different for three typical heavy-  
16 pollution episodes, which belong to three distinct pollution types. The  $PM_{2.5}$  concentrations in  
17 the first episode (“Local” type) are dominated by local sources and primary  $PM_{2.5}$  emissions,  
18 while the second episode (“South” type) is primarily affected by precursor emissions from  
19 local and southern regions. The third episode (“Southeast” type) is significantly influenced by  
20 emissions of both primary inorganic  $PM_{2.5}$  and precursors from multiple regions. Future  
21 investigations are needed to acquire generalized patterns for the source contributions of  
22 various heavy-pollution types.

23 The results of the present study have important implications for  $PM_{2.5}$  control policies  
24 over the BTH region. First, the controls of primary  $PM_{2.5}$  emissions should be a priority in  
25  $PM_{2.5}$  control strategies. Primary  $PM_{2.5}$ , including primary inorganic  $PM_{2.5}$  and POA,  
26 contribute over half of the 4-month mean  $PM_{2.5}$  concentrations, which is even higher in the  
27 winter when heavy pollution frequently occurs. The industry sector and the residential and  
28 commercial sectors represent 85% of the total primary  $PM_{2.5}$  emissions, and therefore should  
29 be the focus of primary  $PM_{2.5}$  controls. In particular, we should pay special attention to the  
30 residential and commercial sectors, which account for half of the total contribution of primary  
31  $PM_{2.5}$  emissions to  $PM_{2.5}$  concentrations in the winter but have been frequently neglected in  
32 China’s previous control policies. Second, the control policies for NMVOC and IVOC

1 emissions should be strengthened. The sensitivity of PM<sub>2.5</sub> concentrations to NMVOC+IVOC  
2 is one of the largest among all precursors. In particular, the controls of NMVOC and IVOC  
3 emissions are very effective for PM<sub>2.5</sub> reduction even at the initial control stage, as indicated  
4 by the large sensitivity at small reduction ratios. Moreover, NMVOC reduction is also crucial  
5 for the mitigation of O<sub>3</sub> pollution considering a NMVOC-limited regime over the urban and  
6 its surrounding areas (Xing et al., 2011). Third, NO<sub>x</sub> emissions should be substantially  
7 reduced in both the BTH and other parts of China; in the long run, the reduction ratio should  
8 preferably approach their maximum feasible reduction levels. Fourth, more stringent control  
9 policies should be enforced in Southern Hebei, which on one hand suffers from the most  
10 severe PM<sub>2.5</sub> pollution (Wang et al., 2014b), and on the other hand, significantly affects both  
11 local and regional PM<sub>2.5</sub> concentrations. Last but not least, considering the distinct source  
12 contributions in different heavy pollution episodes, episode-specific temporary control  
13 strategies should be formulated according to the source contribution feature of the specific  
14 pollution type.

15 The present study has a few limitations. First, the establishment of ERSM requires several  
16 hundred or over 1000 emission scenarios, although the scenario number needed for a specific  
17 number of control variables has already been dramatically reduced as compared to the  
18 conventional RSM technique. Studies are needed to further reduce the scenario number but  
19 retain the accuracy of the ERSM technique. Second, the current ERSM is developed based on  
20 the meteorological conditions simulated for the base year, and has not considered the impact  
21 of inter-annual variations in meteorological conditions on the relationships between emissions  
22 and PM<sub>2.5</sub> concentrations. Third, although the ERSM-predicted responses of PM<sub>2.5</sub>  
23 concentrations to precursor emissions have been demonstrated to agree well with chemical  
24 transport model simulations, evaluating the predicted responses against the actual situation in  
25 the real atmosphere still represents a major challenge, because it is extremely difficult to  
26 artificially perturb emissions in the atmosphere. Last but not the least, the NMVOC and IVOC  
27 emissions have been lumped together in this study to reduce the number of control variables.  
28 Considering their differences in sources and SOA formation potentials (Jathar et al., 2014;  
29 Wu et al., 2017), a detailed quantification of the individual contributions of NMVOC and  
30 IVOC emissions from various sources to PM<sub>2.5</sub> concentrations is required in the future to  
31 better inform NMVOC/IVOC control policies.

32

1

## 2 **Acknowledgements**

3 This research has been supported by National Science Foundation of China (21625701 &  
4 21521064), MOST National Key R & D program (2016YFC0207601), Strategic Pilot Project  
5 of Chinese Academy of Sciences (XDB05030401), the UCLA Sustainable Los Angeles  
6 Grand Challenge 2016 YZ-50958, and the Jet Propulsion Laboratory, California Institute of  
7 Technology, under contract with NASA. The simulations were completed on the “Explorer  
8 100” cluster system of Tsinghua National Laboratory for Information Science and  
9 Technology.

10

## 11 **References**

- 12 Burnett, R. T., Pope, C. A., Ezzati, M., Olives, C., Lim, S. S., Mehta, S., Shin, H. H., Singh,  
13 G., Hubbell, B., Brauer, M., Anderson, H. R., Smith, K. R., Balmes, J. R., Bruce, N. G.,  
14 Kan, H. D., Laden, F., Pruss-Ustun, A., Michelle, C. T., Gapstur, S. M., Diver, W. R.,  
15 and Cohen, A.: An Integrated Risk Function for Estimating the Global Burden of  
16 Disease Attributable to Ambient Fine Particulate Matter Exposure, *Environ Health*  
17 *Persp*, 122, 397-403, Doi 10.1289/Ehp.1307049, 2014.
- 18 Cai, S. Y., Wang, Y. J., Zhao, B., Wang, S. X., Chang, X., and Hao, J. M.: The impact of the  
19 "Air Pollution Prevention and Control Action Plan" on PM<sub>2.5</sub> concentrations in Jing-  
20 Jin-Ji region during 2012-2020, *Sci. Total. Environ.*, in press, DOI  
21 10.1016/j.scitotenv.2016.11.188, 2016.
- 22 Cheng, I., Zhang, L., Blanchard, P., Dalziel, J., and Tordon, R.: Concentration-weighted  
23 trajectory approach to identifying potential sources of speciated atmospheric mercury at  
24 an urban coastal site in Nova Scotia, Canada, *Atmos Chem Phys*, 13, 6031-6048,  
25 10.5194/acp-13-6031-2013, 2013.
- 26 Cheng, Y. F., Zheng, G. J., Wei, C., Mu, Q., Zheng, B., Wang, Z. B., Gao, M., Zhang, Q., He,  
27 K. B., Carmichael, G., Pöschl, U., and Su, H.: Reactive nitrogen chemistry in aerosol  
28 water as a source of sulfate during haze events in China, *Sci Adv*, 2, e1601530, DOI:  
29 10.1126/sciadv.1601530, 2016.
- 30 Dong, X. Y., Li, J., Fu, J. S., Gao, Y., Huang, K., and Zhuang, G. S.: Inorganic aerosols  
31 responses to emission changes in Yangtze River Delta, China, *Sci Total Environ*, 481,  
32 522-532, DOI 10.1016/j.scitotenv.2014.02.076, 2014.
- 33 Fu, X., Wang, S. X., Zhao, B., Xing, J., Cheng, Z., Liu, H., and Hao, J. M.: Emission  
34 inventory of primary pollutants and chemical speciation in 2010 for the Yangtze River  
35 Delta region, China, *Atmos Environ*, 70, 39-50, DOI 10.1016/j.atmosenv.2012.12.034,  
36 2013.
- 37 Fu, X., Wang, S. X., Chang, X., Cai, S. Y., Xing, J., and Hao, J. M.: Modeling analysis of  
38 secondary inorganic aerosols over China: pollution characteristics, and meteorological  
39 and dust impacts, *Sci Rep-Uk*, 6, 10.1038/srep35992, 2016.
- 40 Gordon, T. D., Presto, A. A., May, A. A., Nguyen, N. T., Lipsky, E. M., Donahue, N. M.,  
41 Gutierrez, A., Zhang, M., Maddox, C., Rieger, P., Chattopadhyay, S., Maldonado, H.,  
42 Maricq, M. M., and Robinson, A. L.: Secondary organic aerosol formation exceeds

1 primary particulate matter emissions for light-duty gasoline vehicles, *Atmos Chem Phys*,  
2 14, 4661-4678, DOI 10.5194/acp-14-4661-2014, 2014a.

3 Gordon, T. D., Presto, A. A., Nguyen, N. T., Robertson, W. H., Na, K., Sahay, K. N., Zhang,  
4 M., Maddox, C., Rieger, P., Chattopadhyay, S., Maldonado, H., Maricq, M. M., and  
5 Robinson, A. L.: Secondary organic aerosol production from diesel vehicle exhaust:  
6 impact of aftertreatment, fuel chemistry and driving cycle, *Atmos Chem Phys*, 14, 4643-  
7 4659, DOI 10.5194/acp-14-4643-2014, 2014b.

8 Guenther, A., Karl, T., Harley, P., Wiedinmyer, C., Palmer, P. I., and Geron, C.: Estimates of  
9 global terrestrial isoprene emissions using MEGAN (Model of Emissions of Gases and  
10 Aerosols from Nature), *Atmos Chem Phys*, 6, 3181-3210, 2006.

11 Hakami, A., Seinfeld, J. H., Chai, T. F., Tang, Y. H., Carmichael, G. R., and Sandu, A.:  
12 Adjoint sensitivity analysis of ozone nonattainment over the continental United States,  
13 *Environ Sci Technol*, 40, 3855-3864, DOI 10.1021/Es052135g, 2006.

14 Han, X., Zhang, M. G., Zhu, L. Y., and Skorokhod, A.: Assessment of the impact of  
15 emissions reductions on air quality over North China Plain, *Atmos Pollut Res*, 7, 249-  
16 259, 10.1016/j.apr.2015.09.009, 2016.

17 Hennigan, C. J., Miracolo, M. A., Engelhart, G. J., May, A. A., Presto, A. A., Lee, T.,  
18 Sullivan, A. P., McMeeking, G. R., Coe, H., Wold, C. E., Hao, W. M., Gilman, J. B.,  
19 Kuster, W. C., de Gouw, J., Schichtel, B. A., Collett, J. L., Kreidenweis, S. M., and  
20 Robinson, A. L.: Chemical and physical transformations of organic aerosol from the  
21 photo-oxidation of open biomass burning emissions in an environmental chamber,  
22 *Atmos Chem Phys*, 11, 7669-7686, DOI 10.5194/acp-11-7669-2011, 2011.

23 Iman, R. L., Davenport, J. M., and Zeigler, D. K.: Latin Hypercube Sampling (Program User's  
24 Guide), Sandia National Laboratories, Albuquerque, NM, U.S., 78 pp., 1980.

25 IPCC: Climate Change 2013: The Physical Science Basis. Contribution of Working Group I  
26 to the Fifth Assessment Report of the Intergovernmental Panel on Climate Change,  
27 edited by: Stocker, T. F., Qin, D., Plattner, G.-K., Tignor, M., Allen, S. K., Boschung, J.,  
28 Nauels, A., Xia, Y., Bex, V., and Midgley, P. M., Cambridge University Press,  
29 Cambridge, United Kingdom and New York, NY, USA, 1535 pp., 2013.

30 Jathar, S. H., Gordon, T. D., Hennigan, C. J., Pye, H. O. T., Pouliot, G., Adams, P. J.,  
31 Donahue, N. M., and Robinson, A. L.: Unspeciated organic emissions from combustion  
32 sources and their influence on the secondary organic aerosol budget in the United States,  
33 *P Natl Acad Sci USA*, 111, 10473-10478, DOI 10.1073/pnas.1323740111, 2014.

34 Jia, Y. T., Rahn, K. A., He, K. B., Wen, T. X., and Wang, Y. S.: A novel technique for  
35 quantifying the regional component of urban aerosol solely from its sawtooth cycles, *J*  
36 *Geophys Res-Atmos*, 113, 10.1029/2008jd010389, 2008.

37 Li, J. W., and Han, Z. W.: A modeling study of severe winter haze events in Beijing and its  
38 neighboring regions, *Atmos Res*, 170, 87-97, 10.1016/j.atmosres.2015.11.009, 2016.

39 Li, M., Zhang, Q., Kurokawa, J., Woo, J. H., He, K. B., Lu, Z., Ohara, T., Song, Y., Streets, D.  
40 G., Carmichael, G. R., Cheng, Y. F., Hong, C. P., Huo, H., Jiang, X. J., Kang, S. C., Liu,  
41 F., Su, H., and Zheng, B.: MIX: a mosaic Asian anthropogenic emission inventory for  
42 the MICS-Asia and the HTAP projects, *Atmos Chem Phys Discuss*, 15, 34813-34869,  
43 doi:10.5194/acpd-15-34813-2015, 2015a.

44 Li, X., Zhang, Q., Zhang, Y., Zheng, B., Wang, K., Chen, Y., Wallington, T. J., Han, W. J.,  
45 Shen, W., Zhang, X. Y., and He, K. B.: Source contributions of urban PM<sub>2.5</sub> in the  
46 Beijing-Tianjin-Hebei region: Changes between 2006 and 2013 and relative impacts of  
47 emissions and meteorology, *Atmos Environ*, 123, 229-239,  
48 10.1016/j.atmosenv.2015.10.048, 2015b.

- 1 Lim, S. S., Vos, T., Flaxman, A. D., Danaei, G., Shibuya, K., Adair-Rohani, H., AlMazroa, M.  
2 A., Amann, M., Anderson, H. R., Andrews, K. G., Aryee, M., Atkinson, C., Bacchus, L.  
3 J., Bahalim, A. N., Balakrishnan, K., Balmes, J., Barker-Collo, S., Baxter, A., Bell, M.  
4 L., Blore, J. D., Blyth, F., Bonner, C., Borges, G., Bourne, R., Boussinesq, M., Brauer,  
5 M., Brooks, P., Bruce, N. G., Brunekreef, B., Bryan-Hancock, C., Bucello, C.,  
6 Buchbinder, R., Bull, F., Burnett, R. T., Byers, T. E., Calabria, B., Carapetis, J.,  
7 Carnahan, E., Chafe, Z., Charlson, F., Chen, H., Chen, J. S., Cheng, A. T.-A., Child, J.  
8 C., Cohen, A., Colson, K. E., Cowie, B. C., Darby, S., Darling, S., Davis, A.,  
9 Degenhardt, L., Dentener, F., Des Jarlais, D. C., Devries, K., Dherani, M., Ding, E. L.,  
10 Dorsey, E. R., Driscoll, T., Edmond, K., Ali, S. E., Engell, R. E., Erwin, P. J., Fahimi, S.,  
11 Falder, G., Farzadfar, F., Ferrari, A., Finucane, M. M., Flaxman, S., Fowkes, F. G. R.,  
12 Freedman, G., Freeman, M. K., Gakidou, E., Ghosh, S., Giovannucci, E., Gmel, G.,  
13 Graham, K., Grainger, R., Grant, B., Gunnell, D., Gutierrez, H. R., Hall, W., Hoek, H.  
14 W., Hogan, A., Hosgood Iii, H. D., Hoy, D., Hu, H., Hubbell, B. J., Hutchings, S. J.,  
15 Ibeanusi, S. E., Jacklyn, G. L., Jasrasaria, R., Jonas, J. B., Kan, H., Kanis, J. A.,  
16 Kassebaum, N., Kawakami, N., Khang, Y.-H., Khatibzadeh, S., Khoo, J.-P., Kok, C.,  
17 Laden, F., Lalloo, R., Lan, Q., Lathlean, T., Leasher, J. L., Leigh, J., Li, Y., Lin, J. K.,  
18 Lipshultz, S. E., London, S., Lozano, R., Lu, Y., Mak, J., Malekzadeh, R., Mallinger, L.,  
19 Marcenes, W., March, L., Marks, R., Martin, R., McGale, P., McGrath, J., Mehta, S.,  
20 Memish, Z. A., Mensah, G. A., Merriman, T. R., Micha, R., Michaud, C., Mishra, V.,  
21 Hanafiah, K. M., Mokdad, A. A., Morawska, L., Mozaffarian, D., Murphy, T., Naghavi,  
22 M., Neal, B., Nelson, P. K., Nolla, J. M., Norman, R., Olives, C., Omer, S. B., Orchard,  
23 J., Osborne, R., Ostro, B., Page, A., Pandey, K. D., Parry, C. D. H., Passmore, E., Patra,  
24 J., Pearce, N., Pelizzari, P. M., Petzold, M., Phillips, M. R., Pope, D., Pope Iii, C. A.,  
25 Powles, J., Rao, M., Razavi, H., Rehfuss, E. A., Rehm, J. T., Ritz, B., Rivara, F. P.,  
26 Roberts, T., Robinson, C., Rodriguez-Portales, J. A., Romieu, I., Room, R., Rosenfeld,  
27 L. C., Roy, A., Rushton, L., Salomon, J. A., Sampson, U., Sanchez-Riera, L., Sanman,  
28 E., Sapkota, A., Seedat, S., Shi, P., Shield, K., Shivakoti, R., Singh, G. M., Sleet, D. A.,  
29 Smith, E., Smith, K. R., Stapelberg, N. J. C., Steenland, K., Stöckl, H., Stovner, L. J.,  
30 Straif, K., Straney, L., Thurston, G. D., Tran, J. H., Van Dingenen, R., van Donkelaar,  
31 A., Veerman, J. L., Vijayakumar, L., Weintraub, R., Weissman, M. M., White, R. A.,  
32 Whiteford, H., Wiersma, S. T., Wilkinson, J. D., Williams, H. C., Williams, W., Wilson,  
33 N., Woolf, A. D., Yip, P., Zielinski, J. M., Lopez, A. D., Murray, C. J. L., and Ezzati,  
34 M.: A comparative risk assessment of burden of disease and injury attributable to 67 risk  
35 factors and risk factor clusters in 21 regions, 1990–2010: a systematic analysis for the  
36 Global Burden of Disease Study 2010, *The Lancet*, 380, 2224-2260,  
37 [http://dx.doi.org/10.1016/S0140-6736\(12\)61766-8](http://dx.doi.org/10.1016/S0140-6736(12)61766-8), 2012.
- 38 Liu, J., Mauzerall, D. L., Chen, Q., Zhang, Q., Song, Y., Peng, W., Klimont, Z., Qiu, X. H.,  
39 Zhang, S. Q., Hu, M., Lin, W. L., Smith, K. R., and Zhu, T.: Air pollutant emissions  
40 from Chinese households: A major and underappreciated ambient pollution source, *P*  
41 *Natl Acad Sci USA*, 113, 7756-7761, 10.1073/pnas.1604537113, 2016.
- 42 Lv, L. Y., and Li, H. Y.: Economic evaluation of the health effect of PM10 and PM2.5  
43 pollution over the Beijing-Tianjin-Hebei region, *Acta Scientiarum Naturalium*  
44 *Universitatis Nankaiensis*, 69-77, 2016.
- 45 Qin, Y., and Xie, S. D.: Historical estimation of carbonaceous aerosol emissions from  
46 biomass open burning in China for the period 1990-2005, *Environ Pollut*, 159, 3316-  
47 3323, DOI 10.1016/j.envpol.2011.08.042, 2011.



- 1 Russell, A., Milford, J., Bergin, M. S., Mcbride, S., McNair, L., Yang, Y., Stockwell, W. R.,  
2 and Croes, B.: Urban Ozone Control and Atmospheric Reactivity of Organic Gases,  
3 Science, 269, 491-495, DOI 10.1126/science.269.5223.491, 1995.
- 4 Sandu, A., Daescu, D. N., Carmichael, G. R., and Chai, T. F.: Adjoint sensitivity analysis of  
5 regional air quality models, J Comput Phys, 204, 222-252, DOI  
6 10.1016/j.jcp.2004.10.011, 2005.
- 7 Santner, T. J., Williams, B. J., and Notz, W.: The Design and Analysis of Computer  
8 Experiments, Springer Verlag, New York, U.S., 283 pp., 2003.
- 9 Seinfeld, J. H., Bretherton, C., Carslaw, K. S., Coe, H., DeMott, P. J., Dunlea, E. J., Feingold,  
10 G., Ghan, S., Guenther, A. B., Kahn, R., Kraucunas, I., Kreidenweis, S. M., Molina, M.  
11 J., Nenes, A., Penner, J. E., Prather, K. A., Ramanathan, V., Ramaswamy, V., Rasch, P.  
12 J., Ravishankara, A. R., Rosenfeld, D., Stephens, G., and Wood, R.: Improving our  
13 fundamental understanding of the role of aerosol-cloud interactions in the climate  
14 system, P Natl Acad Sci USA, 113, 5781-5790, 10.1073/pnas.1514043113, 2016.
- 15 Stein, A. F., Draxler, R. R., Rolph, G. D., Stunder, B. J. B., Cohen, M. D., and Ngan, F.:  
16 NOAA's HYSPLIT atmospheric transport and dispersion modeling system, B Am  
17 Meteorol Soc, 96, 2059-2077, 10.1175/bams-d-14-00110.1, 2015.
- 18 Streets, D. G., Fu, J. S., Jang, C. J., Hao, J. M., He, K. B., Tang, X. Y., Zhang, Y. H., Wang,  
19 Z. F., Li, Z. P., and Zhang, Q.: Air quality during the 2008 Beijing Olympic Games,  
20 Atmos Environ, 41, 480-492, DOI 10.1016/j.atmosenv.2006.08.046, 2007.
- 21 The State Council of the People's Republic of China: Notice to issue the "Air Pollution  
22 Prevention and Control Action Plan": [http://www.gov.cn/zwggk/2013-  
23 09/12/content\\_2486773.htm](http://www.gov.cn/zwggk/2013-09/12/content_2486773.htm), access: September 9, 2016, 2013.
- 24 U.S. Environmental Protection Agency: Technical support document for the proposed PM  
25 NAAQS rule: Response Surface Modeling[R/OL]:  
26 [http://www.epa.gov/scram001/reports/pmnaaqs\\_tsd\\_rsm\\_all\\_021606.pdf](http://www.epa.gov/scram001/reports/pmnaaqs_tsd_rsm_all_021606.pdf), access: 2015-  
27 02-01, 2006.
- 28 van Donkelaar, A., Martin, R. V., Brauer, M., and Boys, B. L.: Use of satellite observations  
29 for long-term exposure assessment of global concentrations of fine particulate matter,  
30 Environmental health perspectives, 123, 135, 2015.
- 31 Wang, G. H., Zhang, R. Y., Gomez, M. E., Yang, L. X., Zamora, M. L., Hu, M., Lin, Y., Peng,  
32 J. F., Guo, S., Meng, J. J., Li, J. J., Cheng, C. L., Hu, T. F., Ren, Y. Q., Wang, Y. S.,  
33 Gao, J., Cao, J. J., An, Z. S., Zhou, W. J., Li, G. H., Wang, J. Y., Tian, P. F., Marrero-  
34 Ortiz, W., Secrest, J., Du, Z. F., Zheng, J., Shang, D. J., Zeng, L. M., Shao, M., Wang,  
35 W. G., Huang, Y., Wang, Y., Zhu, Y. J., Li, Y. X., Hu, J. X., Pan, B., Cai, L., Cheng, Y.  
36 T., Ji, Y. M., Zhang, F., Rosenfeld, D., Liss, P. S., Duce, R. A., Kolb, C. E., and Molina,  
37 M. J.: Persistent sulfate formation from London Fog to Chinese haze, P Natl Acad Sci  
38 USA, 113, 13630-13635, 10.1073/pnas.1616540113, 2016a.
- 39 Wang, J. D., Wang, S. X., Jiang, J. K., Ding, A. J., Zheng, M., Zhao, B., Wong, D. C., Zhou,  
40 W., Zheng, G. J., Wang, L., Pleim, J. E., and Hao, J. M.: Impact of aerosol-meteorology  
41 interactions on fine particle pollution during China's severe haze episode in January  
42 2013, Environ Res Lett, 9, 094002, DOI 10.1088/1748-9326/9/9/094002, 2014a.
- 43 Wang, J. D., Xing, J., Mathur, R., Pleim, J. E., Wang, S. X., Hogrefe, C., Gan, C.-M., Wong,  
44 D. C., and Hao, J. M.: Historical Trends in PM2.5-Related Premature Mortality during  
45 1990-2010 across the Northern Hemisphere, Environ Health Persp, in press, DOI  
46 10.1289/EHP298, 2016b.
- 47 Wang, J. D., Zhao, B., Wang, S. X., Yang, F. M., Xing, J., Morawska, L., Ding, A. J.,  
48 Kulmala, M., Kerminen, V. M., Kujansuu, J., Wang, Z. F., Ding, D. A., Zhang, X. Y.,

- 1 Wang, H. B., Tian, M., Petaja, T., Jiang, J. K., and Hao, J. M.: Particulate matter  
2 pollution over China and the effects of control policies, *Sci Total Environ*, 584, 426-447,  
3 10.1016/j.scitotenv.2017.01.027, 2017.
- 4 Wang, L. T., Hao, J. M., He, K. B., Wang, S. X., Li, J. H., Zhang, Q., Streets, D. G., Fu, J. S.,  
5 Jang, C. J., Takekawa, H., and Chatani, S.: A modeling study of coarse particulate  
6 matter pollution in Beijing: Regional source contributions and control implications for  
7 the 2008 summer Olympics, *J Air Waste Manage*, 58, 1057-1069, Doi 10.3155/1047-  
8 3289.58.8.1057, 2008.
- 9 Wang, L. T., Jang, C., Zhang, Y., Wang, K., Zhang, Q. A., Streets, D., Fu, J., Lei, Y.,  
10 Schreifels, J., He, K. B., Hao, J. M., Lam, Y. F., Lin, J., Meskhidze, N., Voorhees, S.,  
11 Evarts, D., and Phillips, S.: Assessment of air quality benefits from national air pollution  
12 control policies in China. Part II: Evaluation of air quality predictions and air quality  
13 benefits assessment, *Atmos Environ*, 44, 3449-3457, DOI  
14 10.1016/j.atmosenv.2010.05.058, 2010.
- 15 Wang, L. T., Wei, Z., Yang, J., Zhang, Y., Zhang, F. F., Su, J., Meng, C. C., and Zhang, Q.:  
16 The 2013 severe haze over southern Hebei, China: model evaluation, source  
17 apportionment, and policy implications, *Atmos Chem Phys*, 14, 3151-3173,  
18 10.5194/acp-14-3151-2014, 2014b.
- 19 Wang, S. X., and Zhang, C. Y.: Spatial and temporal distribution of air pollutant emissions  
20 from open burning of crop residues in China, *Sciencepaper Online*, 3, 1-6, 2008.
- 21 Wang, S. X., Xing, J., Jang, C. R., Zhu, Y., Fu, J. S., and Hao, J. M.: Impact assessment of  
22 ammonia emissions on inorganic aerosols in east China using response surface modeling  
23 technique, *Environ Sci Technol*, 45, 9293-9300, DOI 10.1021/Es2022347, 2011.
- 24 Wang, S. X., Zhao, B., Cai, S. Y., Klimont, Z., Nielsen, C. P., Morikawa, T., Woo, J. H., Kim,  
25 Y., Fu, X., Xu, J. Y., Hao, J. M., and He, K. B.: Emission trends and mitigation options  
26 for air pollutants in East Asia, *Atmos Chem Phys*, 14, 6571-6603, DOI 10.5194/acp-14-  
27 6571-2014, 2014c.
- 28 Wang, S. X., Zhao, B., Wu, Y., and Hao, J. M.: Target and measures to prevent and control  
29 ambient fine particle pollution in China, *Chinese Journal of Environmental Management*,  
30 37-43, 2015.
- 31 Wang, Y. J., Bao, S. W., Wang, S. X., Hu, Y. T., Shi, X., Wang, J. D., Zhao, B., Jiang, J. K.,  
32 Zheng, M., Wu, M. H., Russell, A. G., Wang, Y. H., and Hao, J. M.: Local and regional  
33 contributions to fine particulate matter in Beijing during heavy haze episodes, *Sci Total*  
34 *Environ*, in press, DOI: 10.1016/j.scitotenv.2016.12.127, 2016c.
- 35 Wu, W. J.: Health Effect Attributed to Ambient Fine Particle Pollution in the Beijing-Tianjin-  
36 Hebei Region and its Source Apportionment, Doctor, School of Environment, Tsinghua  
37 University, Beijing, China, 98 pp., 2016.
- 38 Wu, W. J., Zhao, B., Wang, S. X., and Hao, J. M.: Ozone and secondary organic aerosol  
39 formation potential from anthropogenic volatile organic compounds emissions in China,  
40 *Journal of Environmental Sciences*, 53, 224-237, 10.1016/j.jes.2016.03.025, 2017.
- 41 Xing, J., Wang, S. X., Jang, C., Zhu, Y., and Hao, J. M.: Nonlinear response of ozone to  
42 precursor emission changes in China: a modeling study using response surface  
43 methodology, *Atmos Chem Phys*, 11, 5027-5044, DOI 10.5194/acp-11-5027-2011,  
44 2011.
- 45 Yang, Y. J., Wilkinson, J. G., and Russell, A. G.: Fast, direct sensitivity analysis of  
46 multidimensional photochemical models, *Environ Sci Technol*, 31, 2859-2868, DOI  
47 10.1021/Es970117w, 1997.

- 1 Ying, Q., Wu, L., and Zhang, H. L.: Local and inter-regional contributions to PM<sub>2.5</sub> nitrate  
2 and sulfate in China, *Atmos Environ*, 94, 582-592, 10.1016/j.atmosenv.2014.05.078,  
3 2014.
- 4 Yu, L. D., Wang, G. F., Zhang, R. J., Zhang, L. M., Song, Y., Wu, B. B., Li, X. F., An, K.,  
5 and Chu, J. H.: Characterization and Source Apportionment of PM<sub>2.5</sub> in an Urban  
6 Environment in Beijing, *Aerosol Air Qual Res*, 13, 574-583, 10.4209/aaqr.2012.07.0192,  
7 2013.
- 8 Zhang, L., Shao, J. Y., Lu, X., Zhao, Y. H., Hu, Y. Y., Henze, D. K., Liao, H., Gong, S. L.,  
9 and Zhang, Q.: Sources and Processes Affecting Fine Particulate Matter Pollution over  
10 North China: An Adjoint Analysis of the Beijing APEC Period, *Environ Sci Technol*, 50,  
11 8731-8740, 10.1021/acs.est.6b03010, 2016.
- 12 Zhang, W., Guo, J. H., Sun, Y. L., Yuan, H., Zhuang, G. S., Zhuang, Y. H., and Hao, Z. P.:  
13 Source apportionment for,urban PM<sub>10</sub> and PM<sub>2.5</sub> in the Beijing area, *Chinese Sci Bull*,  
14 52, 608-615, 10.1007/s11434-007-0076-5, 2007.
- 15 Zhao, B., Wang, S. X., Dong, X. Y., Wang, J. D., Duan, L., Fu, X., Hao, J. M., and Fu, J.:  
16 Environmental effects of the recent emission changes in China: implications for  
17 particulate matter pollution and soil acidification, *Environ Res Lett*, 8, 024031, DOI  
18 10.1088/1748-9326/8/2/024031, 2013a.
- 19 Zhao, B., Wang, S. X., Liu, H., Xu, J. Y., Fu, K., Klimont, Z., Hao, J. M., He, K. B., Cofala,  
20 J., and Amann, M.: NO<sub>x</sub> emissions in China: historical trends and future perspectives,  
21 *Atmos Chem Phys*, 13, 9869-9897, DOI 10.5194/acp-13-9869-2013, 2013b.
- 22 Zhao, B., Wang, S. X., Wang, J. D., Fu, J. S., Liu, T. H., Xu, J. Y., Fu, X., and Hao, J. M.:  
23 Impact of national NO<sub>x</sub> and SO<sub>2</sub> control policies on particulate matter pollution in  
24 China, *Atmos Environ*, 77, 453-463, DOI 10.1016/j.atmosenv.2013.05.012, 2013c.
- 25 Zhao, B., Wang, S. X., Donahue, N. M., Chuang, W., Hildebrandt Ruiz, L., Ng, N. L., Wang,  
26 Y. J., and Hao, J. M.: Evaluation of one-dimensional and two-dimensional volatility  
27 basis sets in simulating the aging of secondary organic aerosols with smog-chamber  
28 experiments, *Environ Sci Technol*, 49, 2245-2254, DOI 10.1021/es5048914, 2015a.
- 29 Zhao, B., Wang, S. X., Xing, J., Fu, K., Fu, J. S., Jang, C., Zhu, Y., Dong, X. Y., Gao, Y., Wu,  
30 W. J., Wang, J. D., and Hao, J. M.: Assessing the nonlinear response of fine particles to  
31 precursor emissions: development and application of an extended response surface  
32 modeling technique v1.0, *Geosci Model Dev*, 8, 115-128, DOI 10.5194/gmd-8-115-  
33 2015, 2015b.
- 34 Zhao, B., Wang, S. X., Donahue, N. M., Jathar, S. H., Huang, X. F., Wu, W. J., Hao, J. M.,  
35 and Robinson, A. L.: Quantifying the effect of organic aerosol aging and intermediate-  
36 volatility emissions on regional-scale aerosol pollution in China, *Sci Rep-Uk*, 6,  
37 10.1038/srep28815, 2016.
- 38 Zhao, B., Liou, K.-N., Gu, Y., Jiang, J. H., Li, Q., Fu, R., Huang, L., Liu, X., Shi, X., Su, H.,  
39 and He, C.: A water vapor modulated aerosol impact on ice crystal size, *Atmos Chem*  
40 *Phys Discuss*, DOI 10.5194/acp-2017-548, DOI 10.5194/acp-2017-548, 2017a.
- 41 Zhao, B., Liou, K. N., Gu, Y., Li, Q. B., Jiang, J. H., Su, H., He, C. L., Tseng, H. L. R., Wang,  
42 S. X., Liu, R., Qi, L., Lee, W. L., and Hao, J. M.: Enhanced PM<sub>2.5</sub> pollution in China  
43 due to aerosol-cloud interactions, *Sci Rep-Uk*, 7, 10.1038/s41598-017-04096-8, 2017b.
- 44 Zhao, Y., Wang, S. X., Duan, L., Lei, Y., Cao, P. F., and Hao, J. M.: Primary air pollutant  
45 emissions of coal-fired power plants in China: Current status and future prediction,  
46 *Atmos Environ*, 42, 8442-8452, DOI 10.1016/j.atmosenv.2008.08.021, 2008.
- 47 Zheng, G. J., Duan, F. K., Su, H., Ma, Y. L., Cheng, Y., Zheng, B., Zhang, Q., Huang, T.,  
48 Kimoto, T., Chang, D., Poschl, U., Cheng, Y. F., and He, K. B.: Exploring the severe

1 winter haze in Beijing: the impact of synoptic weather, regional transport and  
2 heterogeneous reactions, Atmos Chem Phys, 15, 2969-2983, 10.5194/acp-15-2969-2015,  
3 2015.

4

5

6

1 **Tables and figures**

2 Table 1. Description of the RSM/ERSM prediction systems developed in this study.

Method	Control variables	Control scenarios
Conventional RSM technique	5 control variables: total emissions of NO <sub>x</sub> , SO <sub>2</sub> , NH <sub>3</sub> , NMVOC+IVOC, and POA	101 control scenarios: 1) 1 CMAQ/2D-VBS base case; 2) 100 <sup>a</sup> scenarios generated by applying LHS method for the 5 variables.
ERSM technique	55 control variables in total: 11 control variables in each of the 5 regions, including 7 nonlinear control variables, i.e., 1) NO <sub>x</sub> /large point sources (LPS) <sup>b</sup> 2) NO <sub>x</sub> /other sources 3) SO <sub>2</sub> /LPS 4) SO <sub>2</sub> /other sources 5) NH <sub>3</sub> /all sources 6) NMVOC+IVOC/all sources 7) POA/all sources and 4 linear control variables, i.e., 8) Primary inorganic PM <sub>2.5</sub> /power plants 9) Primary inorganic PM <sub>2.5</sub> /Industry 10) Primary inorganic PM <sub>2.5</sub> /residential & commercial 11) Primary inorganic PM <sub>2.5</sub> /transportation	1121 control scenarios: 1) 1 CMAQ/2D-VBS base case; 2) 1000 scenarios, including 200 <sup>a</sup> scenarios generated by applying LHS method for the nonlinear control variables in Beijing, 200 scenarios generated in the same way for Tianjin, 200 scenarios for Northern Hebei, 200 scenarios for Southern Hebei, and 200 scenarios for Eastern Hebei; 3) 100 <sup>a</sup> scenarios generated by applying LHS method for the total emissions of NO <sub>x</sub> , SO <sub>2</sub> , NH <sub>3</sub> , NMVOC+IVOC, and POA; 4) 20 scenarios where one primary inorganic PM <sub>2.5</sub> control variable is set to 0.25 for each scenario.

3 <sup>a</sup> 100 and 200 scenarios are needed for the response surfaces for 5 and 7 variables, respectively (Xing et al.,  
4 2011; Wang et al., 2011).

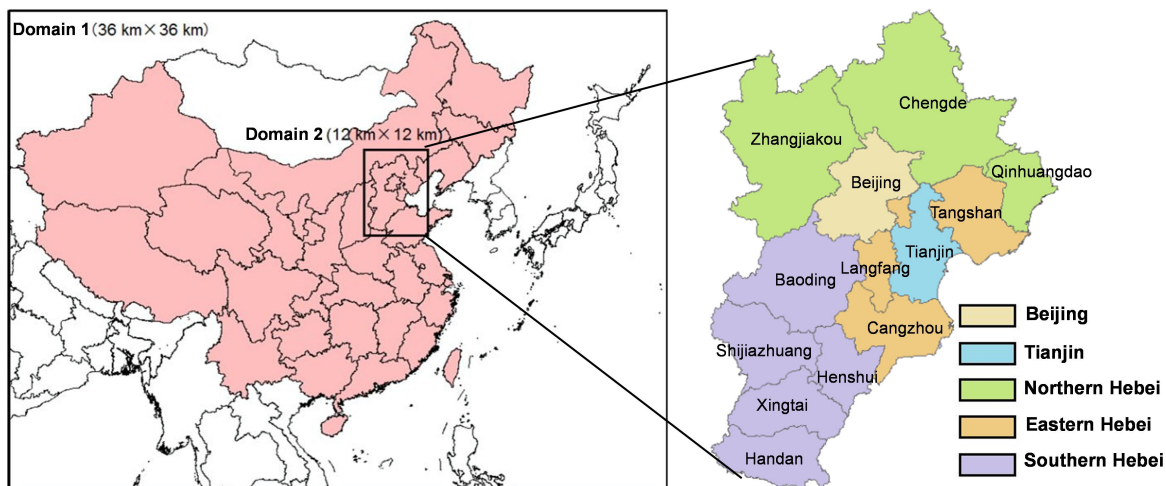
5 <sup>b</sup> LPS includes power plants, iron and steel plants, and cement plants

6

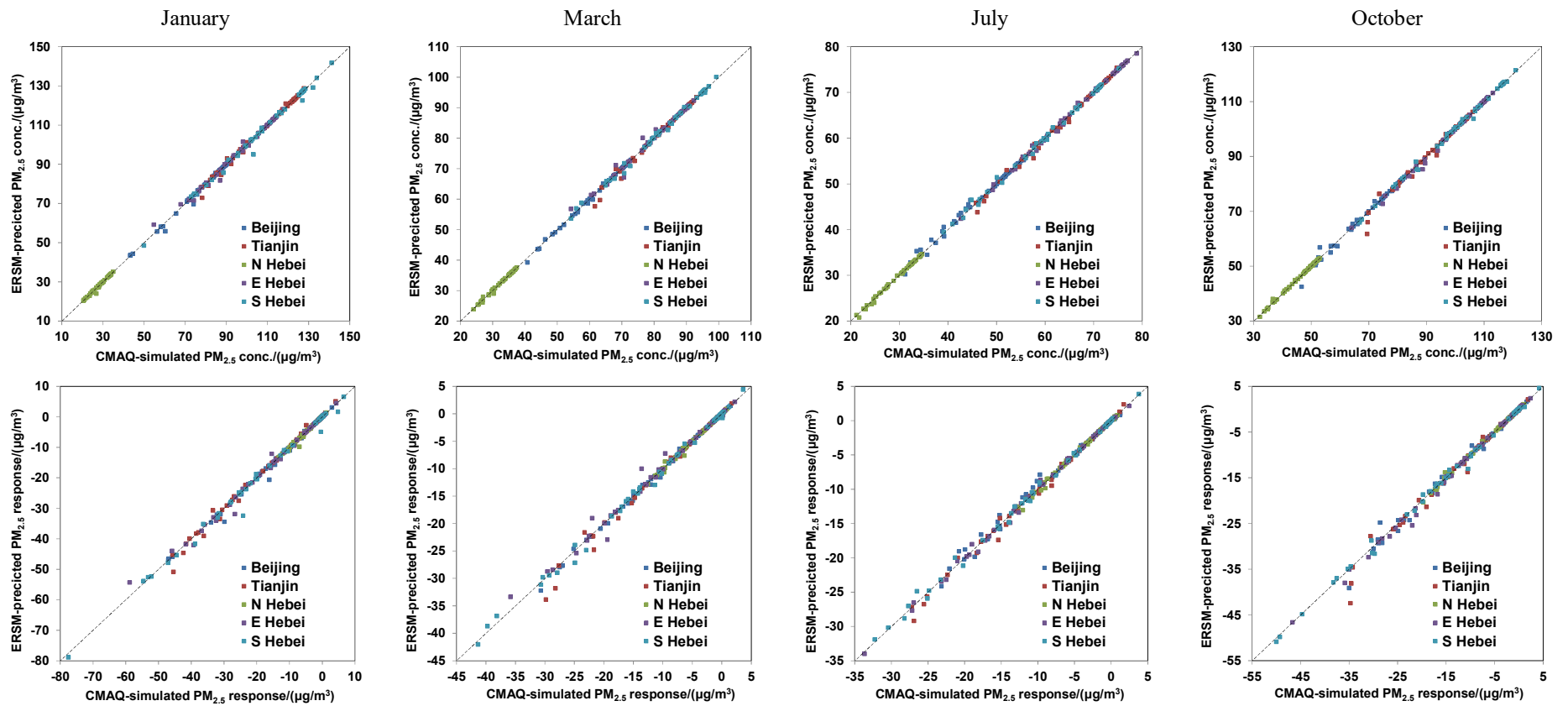
1 Table 2. Comparison between ERSM-predicted and CMAQ/2D-VBS-simulated PM<sub>2.5</sub> concentrations for  
 2 54 out-of-sample scenarios.

Month	Variable	Statistical index	Beijing	Tianjin	Northern Hebei	Eastern Hebei	Southern Hebei	
Jan	PM <sub>2.5</sub> concentration	R	0.998	0.998	0.995	0.997	0.997	
		MNE (%)	0.52	0.55	0.64	0.67	0.60	
		Maximum NE (%)	7.56	6.98	10.67	8.01	8.03	
		95% percentile of NEs (%)	1.61	2.86	2.92	3.46	3.02	
		NME (%)	0.44	0.46	0.57	0.53	0.53	
	PM <sub>2.5</sub> response	R	0.998	0.998	0.995	0.997	0.997	
		NME (%)	3.36	3.48	4.25	4.00	3.88	
	Mar	PM <sub>2.5</sub> concentration	R	0.999	0.996	0.998	0.995	0.999
			MNE (%)	0.37	0.54	0.39	0.57	0.49
			Maximum NE (%)	3.75	6.58	4.30	5.04	3.22
95% percentile of NEs (%)			1.53	3.15	2.03	4.35	2.03	
NME (%)			0.31	0.45	0.34	0.49	0.42	
PM <sub>2.5</sub> response		R	0.999	0.996	0.998	0.995	0.999	
		NME (%)	2.38	4.32	2.70	4.55	3.59	
Jul		PM <sub>2.5</sub> concentration	R	0.997	0.998	0.998	0.999	0.999
			MNE (%)	0.94	0.54	0.46	0.37	0.47
			Maximum NE (%)	5.05	5.02	4.65	1.83	3.62
	95% percentile of NEs (%)		3.47	2.33	2.17	1.49	1.87	
	NME (%)		0.80	0.47	0.41	0.33	0.39	
	PM <sub>2.5</sub> response	R	0.997	0.998	0.998	0.999	0.999	
		NME (%)	4.97	3.71	2.80	2.58	2.78	
	Oct	PM <sub>2.5</sub> concentration	R	0.996	0.994	0.999	0.999	0.999
			MNE (%)	0.83	0.70	0.36	0.39	0.36
			Maximum NE (%)	8.90	11.19	3.79	3.90	2.46
95% percentile of NEs (%)			3.04	3.50	1.44	2.10	1.64	
NME (%)			0.67	0.58	0.30	0.35	0.32	
PM <sub>2.5</sub> response		R	0.996	0.994	0.999	0.999	0.999	
		NME (%)	4.51	5.64	2.20	3.29	2.79	

3

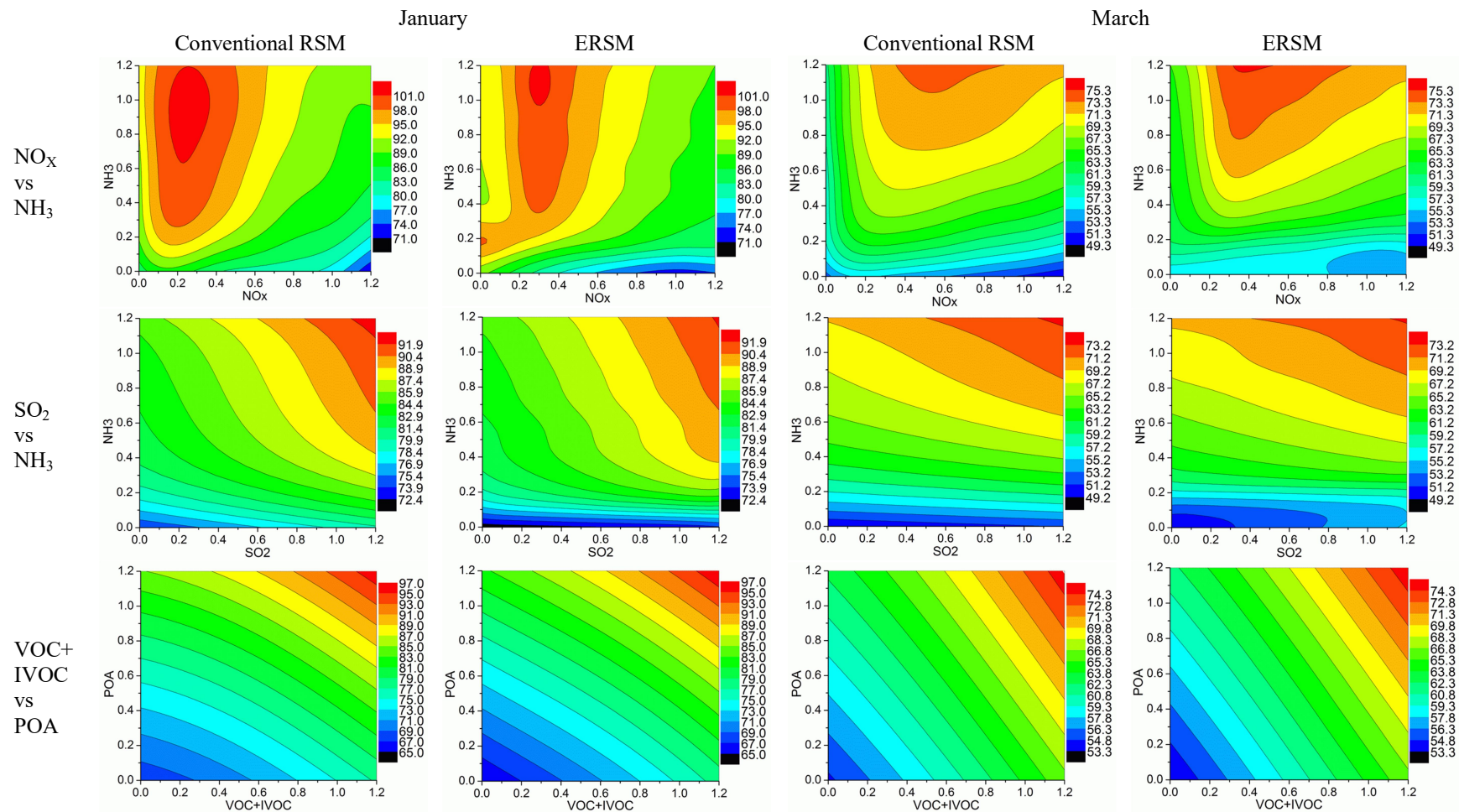


1  
 2 Figure 1. Double nesting domains used in CMAQ/2D-VBS simulation (left) and the definition  
 3 of five target regions in the innermost domain, denoted by different colours (right). The grey  
 4 lines in the right figure represent the boundaries of prefecture-level cities.



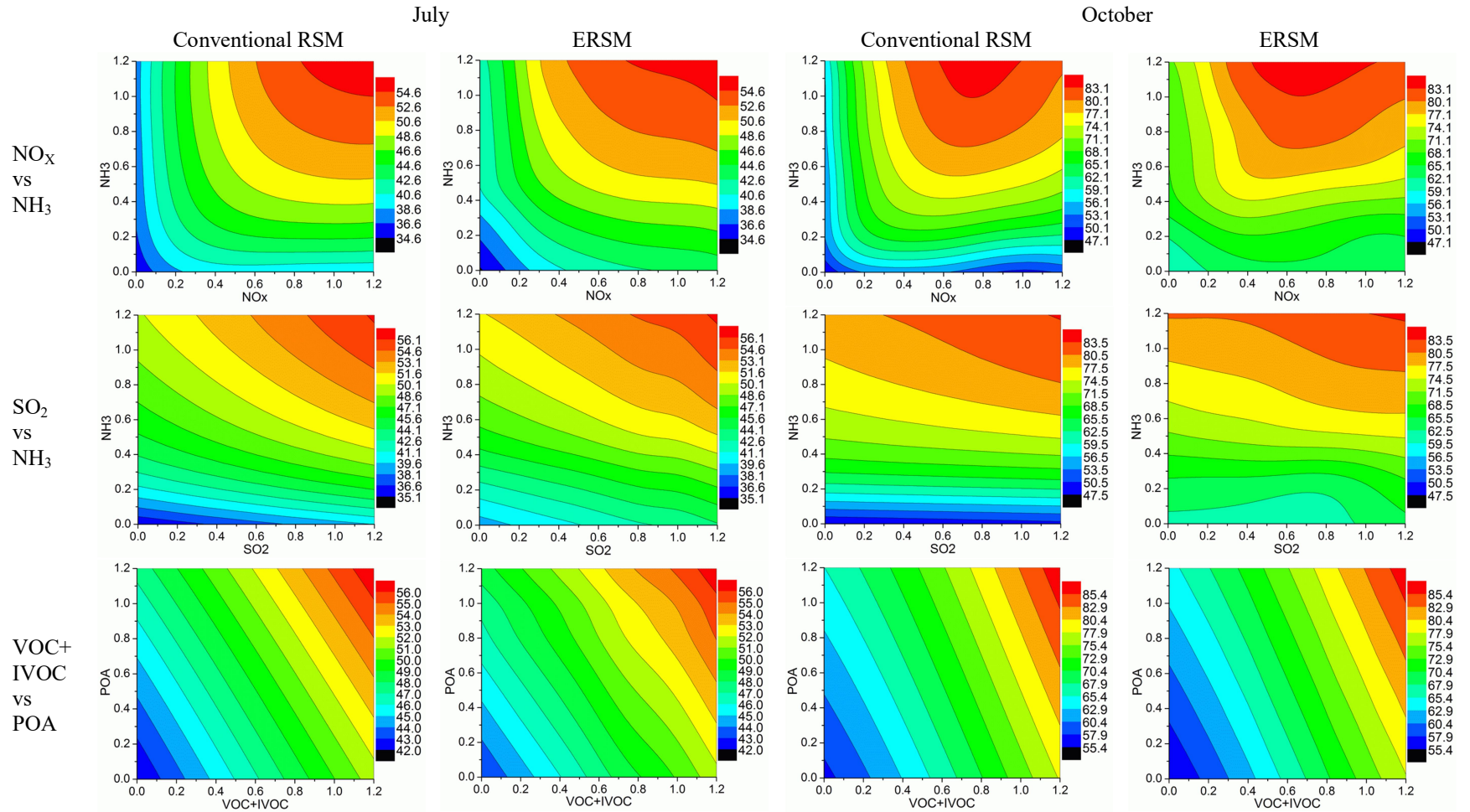
1 Figure 2. Comparison of  $PM_{2.5}$  concentrations (top row) and  $PM_{2.5}$  responses (bottom row) predicted by the ERSM technique with out-of-  
 2 sample CMAQ/2D-VBS simulations. The dashed line is the one-to-one line indicating perfect agreement.



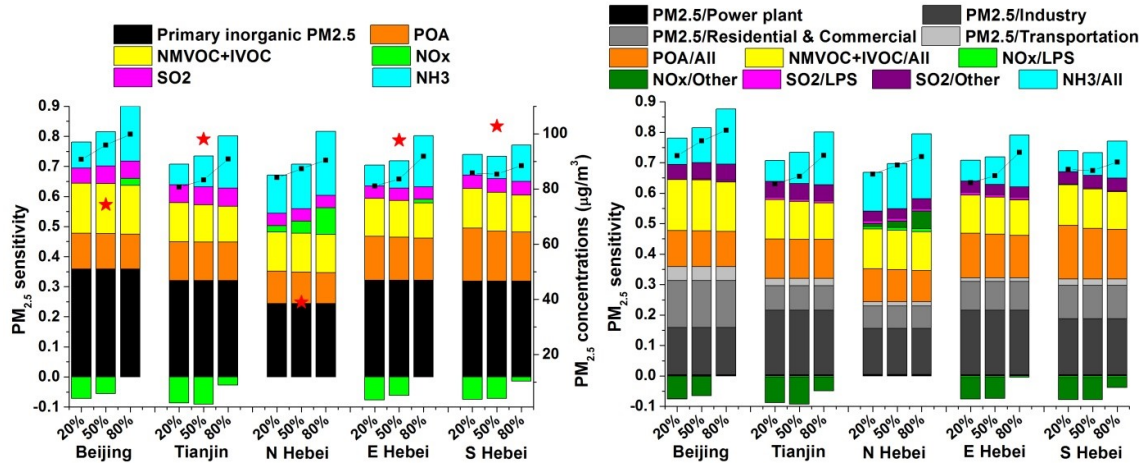


1 Figure 3. Comparison of the 2-D isopleths of  $PM_{2.5}$  concentrations in Beijing in response to the simultaneous changes of precursor  
 2 emissions in all five regions derived from the conventional RSM technique and the ERSM technique. The X- and Y-axis represent the  
 3 emission ratio, defined as the ratios of the changed emissions to the emissions in the base case. The colour contours represent  $PM_{2.5}$   
 4 concentrations (unit:  $\mu g m^{-3}$ ).

1

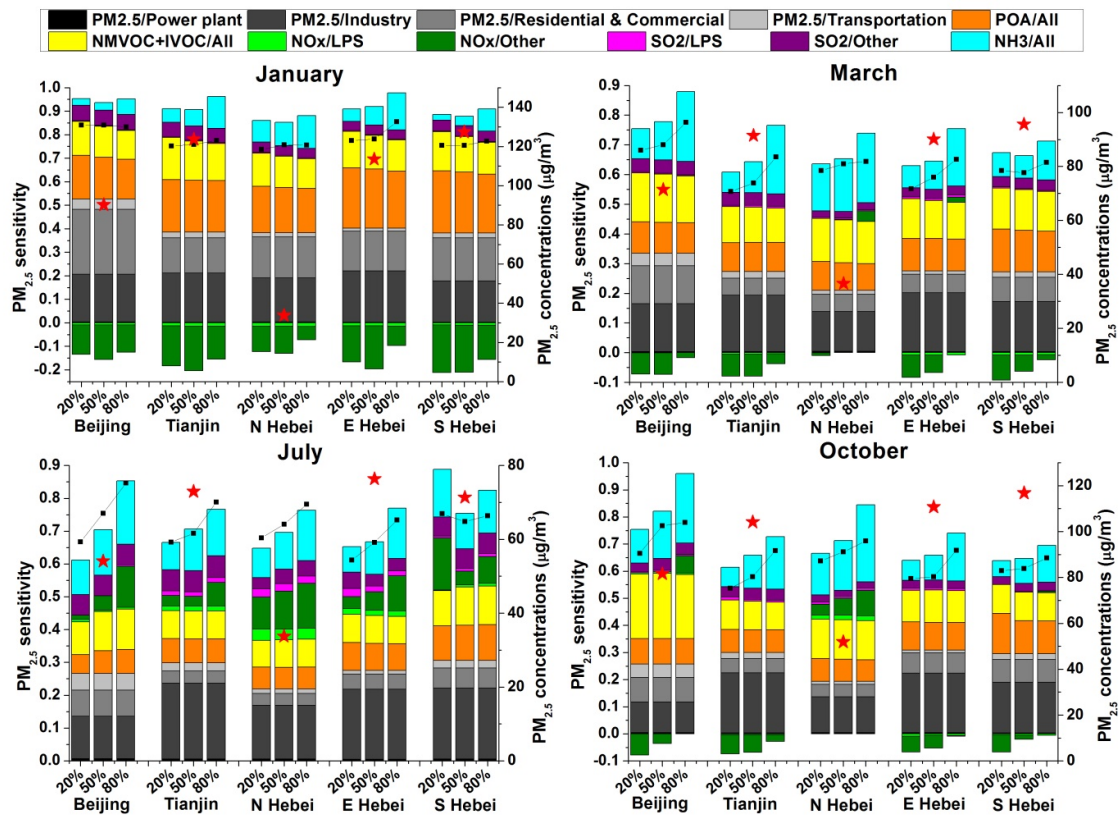


2 Figure 3. Continued.



1  
 2 Figure 4. Sensitivity of 4-month mean  $PM_{2.5}$  concentrations to stepped control of individual  
 3 air pollutants (left) and individual pollutant-sector combinations (right). The X-axis shows the  
 4 reduction ratio ( $= 1 - \text{emission ratio}$ ). The Y-axis shows  $PM_{2.5}$  sensitivity, which is defined as  
 5 the change ratio of concentration divided by the reduction ratio of emissions. The coloured  
 6 bars denote the  $PM_{2.5}$  sensitivities when a particular emission source is controlled while the  
 7 others stay the same as the base case; the black dotted line denotes the  $PM_{2.5}$  sensitivity when  
 8 all emission sources are controlled simultaneously. The red stars represent  $PM_{2.5}$   
 9 concentrations in the base case.

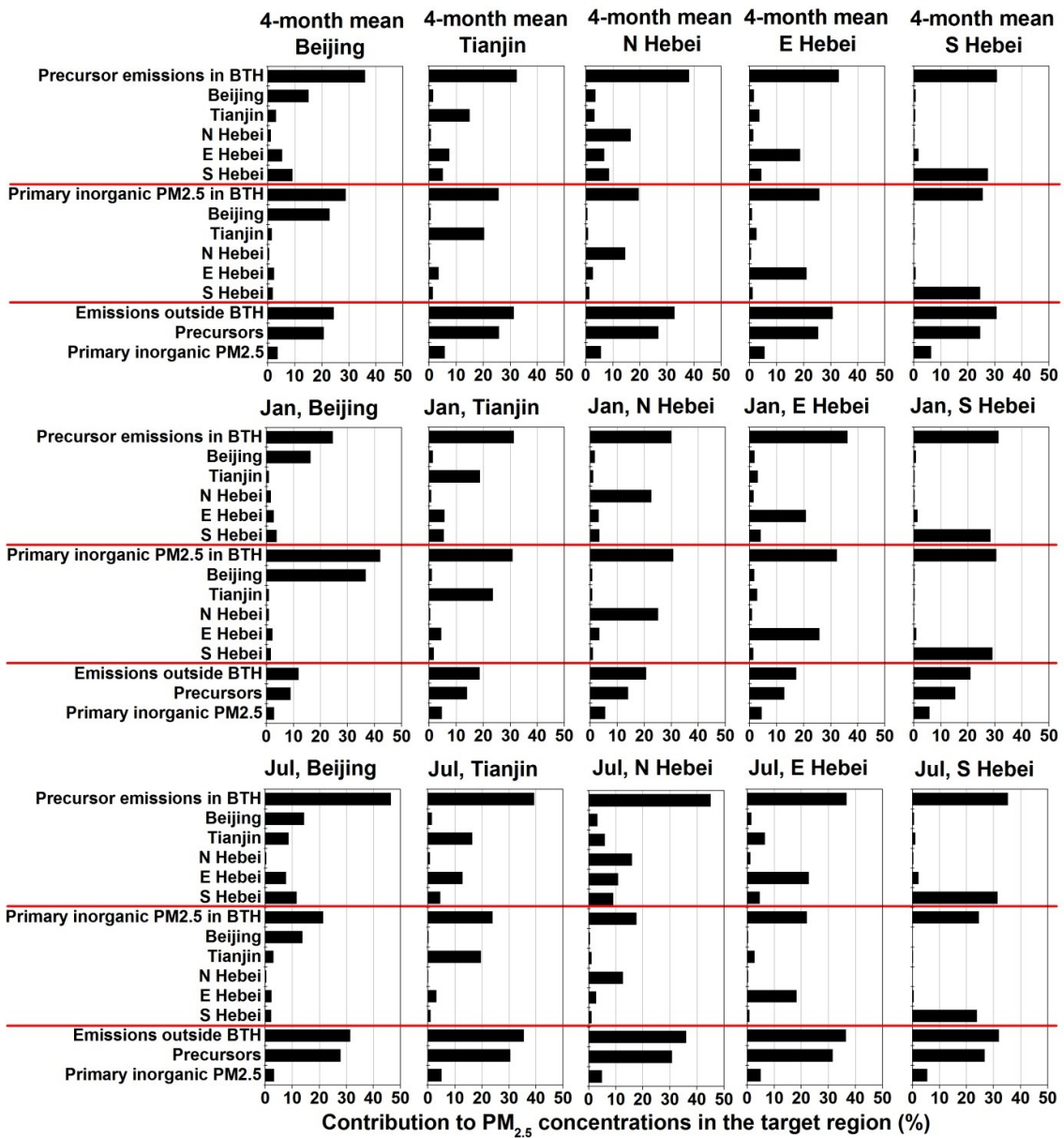
10



1  
 2 Figure 5. Sensitivity of monthly mean  $PM_{2.5}$  concentrations to stepped control of individual  
 3 air pollutants from individual sectors in January, March, July, and October. The meanings of  
 4 X-axis, Y-axis, coloured bars, black dotted lines, and red stars are the same as Fig. 4.

5

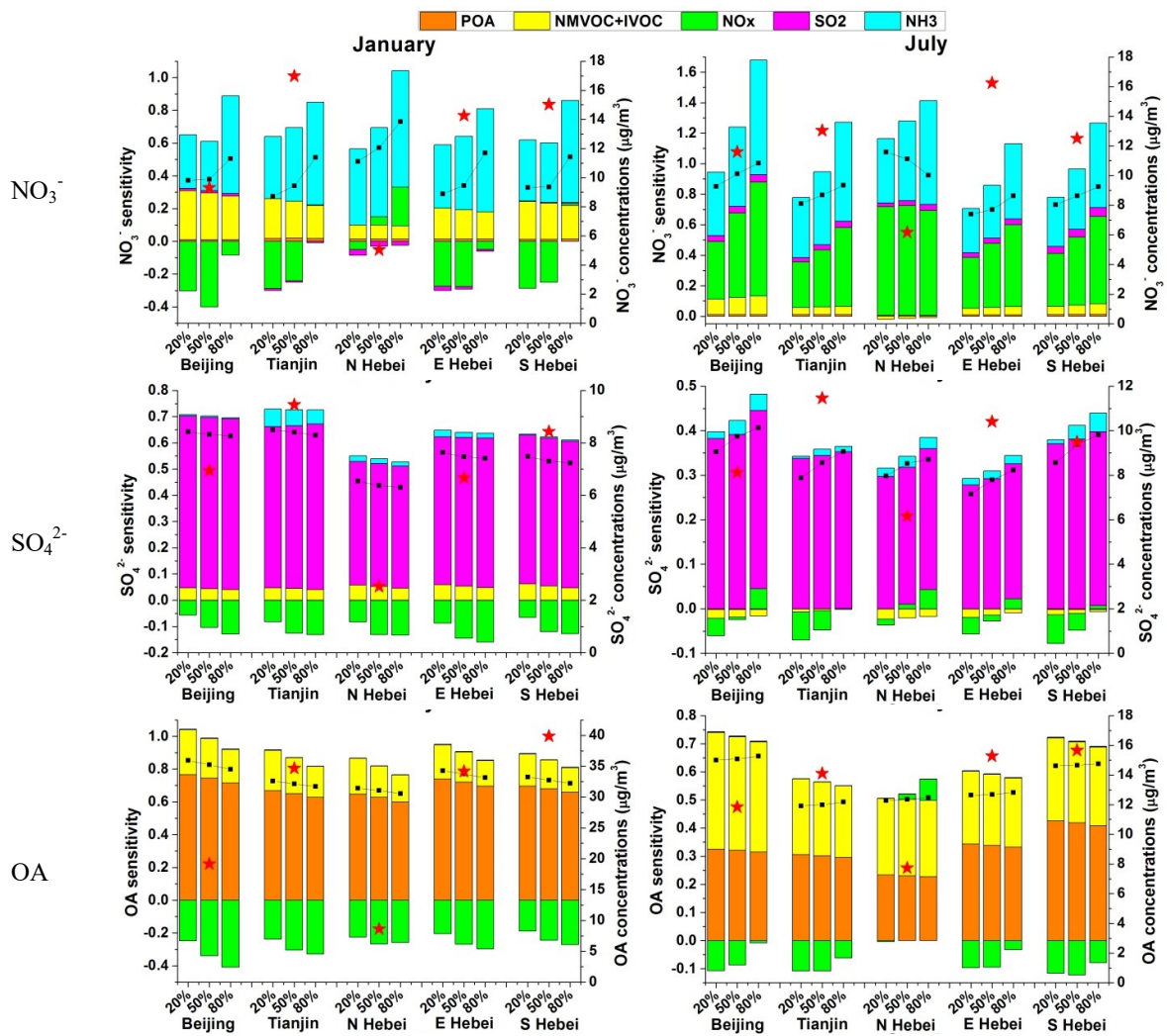




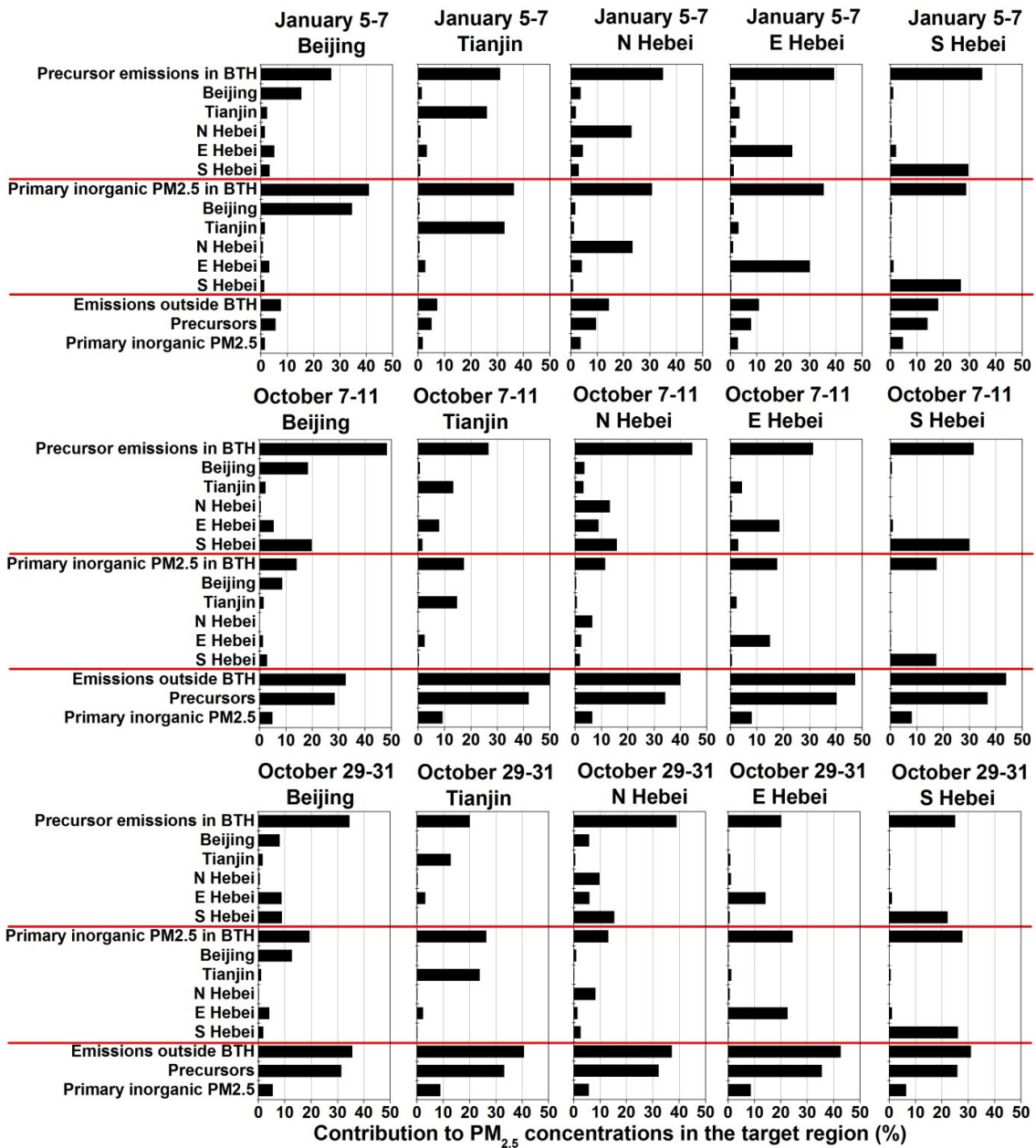
1

2

3 Figure 6. Contributions of precursor (NO<sub>x</sub>, SO<sub>2</sub>, NH<sub>3</sub>, NMVOC, IVOC, and POA) and  
 4 primary inorganic PM<sub>2.5</sub> emissions from individual regions to PM<sub>2.5</sub> concentrations. The  
 5 contributions are quantified by comparing the base case with sensitivity scenarios in which  
 6 emissions from a specific source are reduced by 80%. This figure illustrates contributions to  
 7 4-month mean PM<sub>2.5</sub> concentrations and monthly mean PM<sub>2.5</sub> concentrations in January and  
 8 July. The results for March and October are given in Fig. S6.



1 Figure 7. Sensitivity of monthly mean  $\text{NO}_3^-$ ,  $\text{SO}_4^{2-}$ , and OA concentrations to stepped control  
 2 of individual air pollutants in January and July. The meanings of X-axis, Y-axis, coloured  
 3 bars, black dotted lines, and red stars are the same as Fig. 4 but for  $\text{NO}_3^-/\text{SO}_4^{2-}/\text{OA}$ . The  
 4 results for March and October are given in Fig. S7.  
 5



1

2

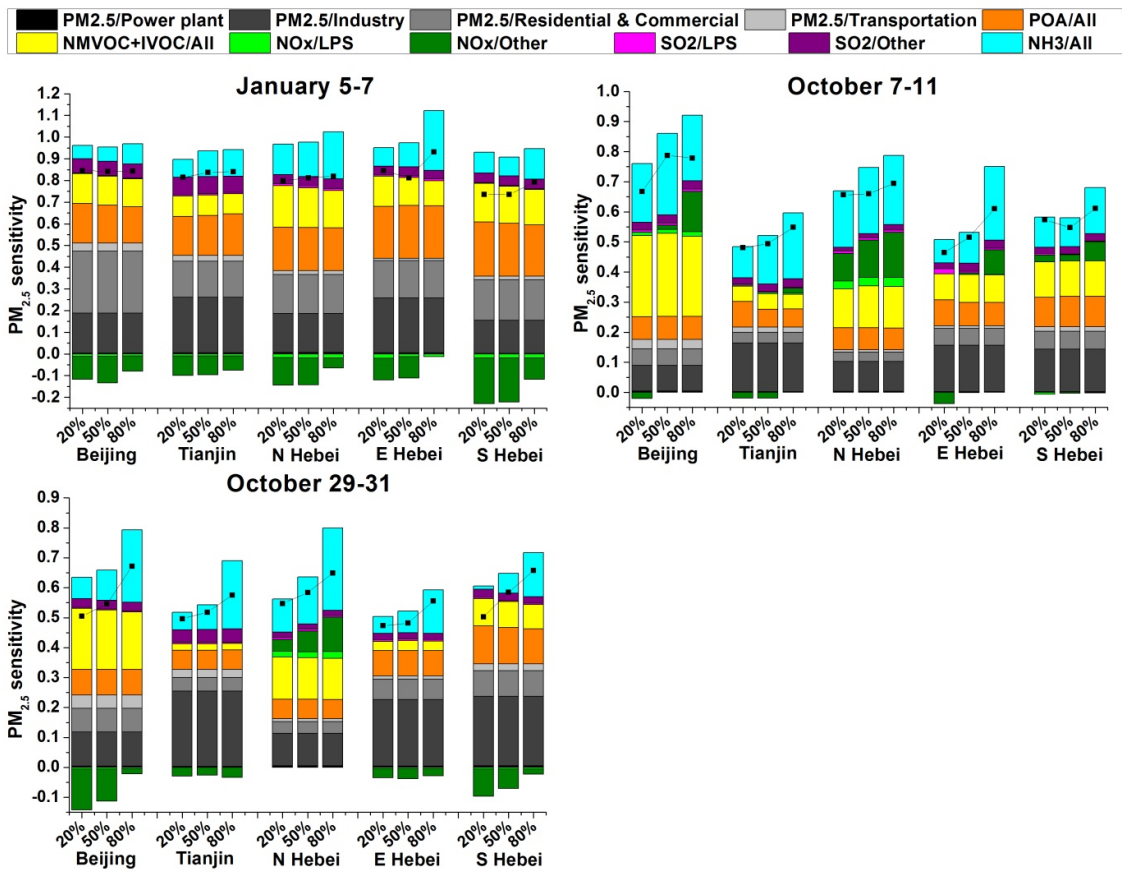
3

4

5

6

Figure 8. Contribution of precursor (NO<sub>x</sub>, SO<sub>2</sub>, NH<sub>3</sub>, NMVOC, IVOC, and POA) and primary inorganic PM<sub>2.5</sub> emissions from individual regions to PM<sub>2.5</sub> concentrations during three typical heavy-pollution episodes.



1  
 2 Figure 9. Sensitivity of  $PM_{2.5}$  concentrations to stepped control of individual air pollutants  
 3 from individual sectors during three heavy-pollution episodes. The meanings of X-axis, Y-  
 4 axis, coloured bars, and black dotted lines are the same as Fig. 4.

5